INL/EXT-18-44496
Revision 0

Advanced Reactor Technologies (ART): Very High Temperature Reactor (VHTR) Research and Development (R&D) Quarterly Report

October, November, and December 2017

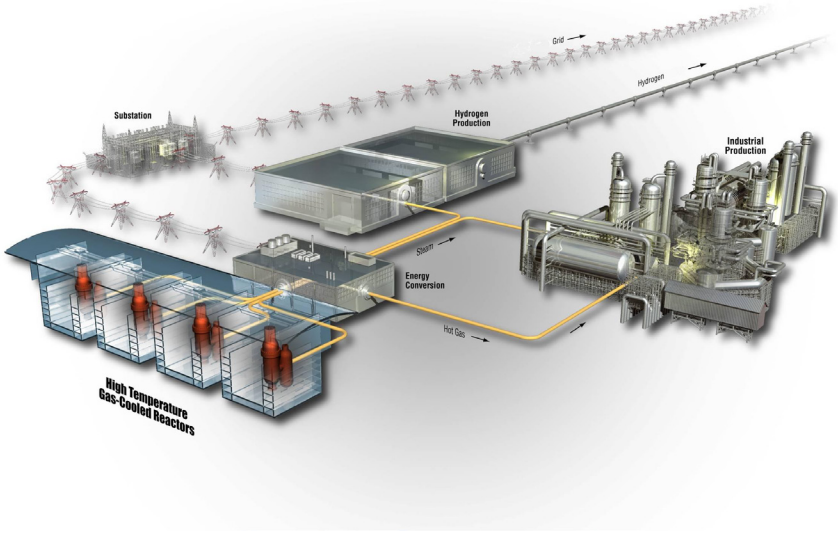

Please note this report contains preliminary data, interim conclusions and observations from work-in-progress.

The INL is a
U.S. Department of Energy
National Laboratory
operated by
Battelle Energy Alliance

Idaho National Laboratory

INL/EXT-18-44496

Revision 0

Advanced Reactor Technologies (ART): Very High Temperature Reactor (VHTR) Research and Development (R&D) Quarterly Report

October, November, and December 2017

Idaho National Laboratory
INL ART TDO Program
Idaho Falls, Idaho 83415

http://www.inl.gov

Prepared for the
U.S. Department of Energy
Office of Nuclear Energy
Under DOE Idaho Operations Office
Contract DE-AC07-05ID14517

INL ART Program

Advanced Reactor Technologies (ART): Very High Temperature Reactor (VHTR) Research and Development (R&D) Quarterly Report

INL/EXT-18-44496

Revision 0

October, November, and December 2017

Approved by

Diane V. Croson
INL ART TDO Deputy Director

2/8/18
Date

CONTENTS

FIGURES

TABLES

ACRONYMS

AG	against grain
AGC	advanced graphite creep
AGR	Advanced Gas Reactor
AMIX	Air/Moisture-Ingress eXperiment
ART	advanced reactor technology
ASME	American Society of Mechanical Engineers
ASTM	ASTM, International (standards organization, formerly American Society for Testing and Materials)
ATR	Advanced Test Reactor
BOL	beginning of life
BP	burnable poison
CCCTF	Core Conduction Cooldown Test Facility
CR	control rod
CRP	Coordinated Research Project
CTE	coefficient of thermal expansion
DLBL	deconsolidation-leach-burn-leach
DOE	Department of Energy
DTF	designed-to-fail
ESA	Experiment Safety Analysis
FACS	fuel accident condition simulator
FIMA	fissions per initial metal atom
FITT	Furnace for Irradiated TRISO-particle Testing
FY	fiscal year
GA	General Atomics
GECT	gamma emission computed tomography
GRS	Gesellschaft für Anlagen- und Reaktorsicherheit
HFEF	Hot Fuel Examination Facility
HOG	HFEF out-of-cell gamma
HT	heat treatment
HTGR	high-temperature gas-cooled reactor
HTM	High Temperature Furnace Module
HTTF	High Temperature Test Facility
IAEA	International Atomic Energy Agency
ICP-MS	inductively coupled plasma mass spectrometry

IMGA	irradiated microsphere gamma analyzer
INL	Idaho National Laboratory
IPyC	inner pyrolytic carbon
LBL	leach-burn-leach
LWR	light-water reactor
MHTGR	modular high-temperature gas-cooled reactor
NDMAS	Nuclear Data Management and Analysis System
NEA	Nuclear Energy Agency
NGNP	Next Generation Nuclear Plant
NRAD	Neutron Radiography Reactor
NRC	Nuclear Regulatory Committee
NSUF	Nuclear Scientific User Facility
OECD	Organization for Economic Cooperation and Development
ORNL	Oak Ridge National Laboratory
PBMR	Pebble-Bed Modular Reactor
PED	precession electron diffraction
PIE	post-irradiation examination
R&D	research and development
RPT	reactivity physical transformation
RSD	relative standard deviation
SAD	selected area diffraction
SATS	Severe Accident Test Station
SCALE	Standardized Computer Analyses for Licensing Evaluation
SD	standard deviation
SEM	scanning electron microscopy
STEM	scanning transmission electron microscopy
TA	time averaged
TAVA	time averaged, volume averaged
TEM	transmission electron microscopy
TRISO	tristructural isotropic
UCO	uranium carbide/oxide
UHP	ultra-high-purity
VHTRC	Very High Temperature Reactor Critical Assembly
WG	with grain
XRD	x-ray diffraction

Advanced Reactor Technologies (ART): Very High Temperature Reactor (VHTR) Research and Development (R&D) Quarterly Report

1. MAJOR ACCOMPLISHMENTS

1.1 Fuels Development

Highlights of Advanced Gas Reactor (AGR) Fuels Development activities during October through December 2017 are as follows:

October

- Completed oxidation (burn) of AGR-2 Capsule 5 graphite compact holder and initiated post-burn leach.
- Completed gamma counting of solutions from AGR-3/4 Compact 12-1 radial deconsolidation leach burn leach (DLBL).
- Completed gamma counting of radial DLBL solutions of AGR-3/4 Compact 12-3.
- Transferred solutions from radial DLBL of AGR-3/4 compacts 12-1, 12-3, and 3-3 out of the Analytical Laboratory (AL) Hot Cell 5 for Sr-90 and inductively coupled plasma mass spectrometry (ICP-MS).
- Completed particle inspection and selection of 30 particles per radial fraction for the 2 radial fractions of AGR-3/4 Compact 12-1, 3 fractions of AGR-3/4 Compact 12-3, and 5 fractions of AGR-3/4 Compact 3-3.
- Initiated gamma counting of selected particles from outer, middle, and axial fraction collected from the radial DLBL of AGR-3/4 Compact 3-3.
- Completed heat tracing and insulation of gas supply, gas analysis, and exhaust lines from development air/moisture ingress furnace.
- Completed scanning transmission electron microscopy and precession electron diffraction (PED) data collection on 2 locations (6 lamellae) from the silicon carbide (SiC) layer and on 2 locations (4 lamellae) of the inner pyrolytic carbon (IPyC)-buffer layer interface of Particle AGR2-222-RS36. Ag was identified on limited locations at the IPyC/SiC interfaces.
- Completed electron probe micro-analyzer research plan maps for Particles AGR2-223-RS034, AGR2-222-RS019 and AGR2-222-RS027.
- Submitted 3 Nuclear Scientific User Facility (NSUF) rapid turnaround experiments covering topics as follows:
    - Atom probe tomography and selected area diffraction (SAD) of uranium carbide/oxide (UCO) kernels from Particles AGR2-223-RS06 and AGR1-632-034.
    - Scanning electron microscopy electron dispersive spectrographic (SEM-EDS) mapping and SAD in UCO kernels from particle AGR1-433-004.
    - In-situ heat up (up to 1200°C) transmission electron microscopy (TEM) studies of fission products in irradiated SiC layers.

- Completed correlation of grain-boundary precipitate chemical compositions with grain-boundary character for the SiC layer from AGR2-223-RS06. Main findings included:
  - Grain-boundary precipitates contained predominantly Pd.
  - Most grain-boundary precipitates were associated with random, high-angle grain boundaries.
  - No precipitates were found on low-angle grain boundaries.
  - A very small fraction of grain-boundary precipitates contained either Zr or Mo in addition to other fission-product elements.
- Observed significant phase differences in the unirradiated kernel changing from primarily UC_2 to UC in the irradiated kernel (AGR1-523-SP01). The high-Z (UC[O] phase) material appeared to be present as two distinct variants containing either Zr or Mo. Xe bubbles were found almost exclusively in the "high-Z" phase, predominantly in the Zr-containing variant. A "low-Z" (UO_2[C]) phase was also identified in which trace amounts of I, Nd, Pr, and/or Eu could be detected.
- AGR-2 compact ceramography article was published in *Nuclear Engineering and Design*, F. J. Rice, J. D. Stempien, and P. A. Demkowicz, "Ceramography of irradiated tristructural isotropic (TRISO) fuel from the AGR-2 experiment," In Press.
- Completed Oak Ridge National Laboratory (ORNL) confirmatory leach-burn-leach (LBL) of AGR-5/6/7 overcoated particles and transferred final solutions to Nuclear Analytical Chemistry for uranium analysis. Eight sample aliquots were subjected to two 24-hour pre-burn leaches, a 72-hour burn at 750°C, and two 24-hour post-burn leaches.
- Initiated deconsolidation of first set of 40%-packing fraction AGR-5/6/7 compacts for ORNL confirmatory LBL analysis.
- Initiated 1600°C safety test of AGR-2 UCO Compact 6-2-2.
- Completed six-hour gamma scans with the irradiated microsphere gamma analyzer (IMGA) of TRISO particles selected from as-irradiated AGR-2 UCO Compact 2-2-1.
- Completed post-burn leach of particles from as-irradiated AGR-2 UCO Compact 2-2-1.
- Completed x-ray tomography of particles from 1700°C safety-tested AGR-2 UO_2 Compact 3-4-1.

November

- Restarted the 1600°C safety test of AGR-2 UCO Compact 6-2-2 to complete the 300-h test after successful repair of the ORNL Core Conduction Cooldown Test Facility (CCCTF) cold-finger insertion system (208 h at 1600°C were completed before the bracket supporting the cold finger became loose and the cold finger could not be inserted).
- Completed heating test with zirconia-surrogate TRISO in the ORNL Furnace for Irradiated TRISO-particle Testing (FITT), and initiated pretest gamma survey with the IMGA of 30 particles deconsolidated from as-irradiated AGR-2 Compact 5-4-2 for the first heating test of irradiated particles in the FITT.
- Completed gamma scanning with the IMGA of particles from the first safety-tested compact containing Pebble-Bed Modular Reactor (PBMR) particles (AGR-2 Compact 4-3-1).
- Completed deconsolidation and pre-burn leaching of as-irradiated AGR-2 PBMR Compact 4-3-2 and separated particles from matrix debris for IMGA.
- Completed gamma and mass spectrometry of solutions from post-burn leach of particles from as-irradiated AGR-2 UCO Compact 2-2-1 and 1700°C safety-tested AGR-2 UO_2 Compact 3-4-1.

- Mounted surrogated AGR-2 particles in-cell at Idaho National Laboratory (INL) as final development work for ceramography of loose AGR-2 particles a multiple planes. Multi-plane analyses will study kernel swelling and buffer layer shrinkage.
- Fabricated tooling for sectioning, grinding and polishing AGR-3/4 compacts.
- Mounted surrogate AGR-3/4 compacts in-cell at INL as final development work for AGR-3/4 compact ceramography, which will use optical microscopy to observe the morphology of designed-to-fail particles.
- Completed upper flange lift motor and associated wiring repair on the fuel accident condition simulator (FACS) furnace.
- Completed hot testing and 1800°C cleanup run in the FACS furnace.
- Loaded AGR-3/4 Compact 3-2 into the FACS furnace for a 1400°C heating test scheduled to start the first full week in December.
- Received and reviewed preliminary gamma spectrometry data from physical sampling of the AGR-3/4 inner ring from Capsule 7. Constructed preliminary fission-product concentration profiles in IR-07.
- Completed specification for Air/Moisture-Ingress eXperiment (AMIX) furnace procurement, and received and reviewed bid proposals from vendors.
- Operated the benchtop air/moisture-ingress development furnace under air/helium and steam/helium mixtures.
- Completed final lab walkdown of air/moisture-ingress development furnace to enable full testing with graphite samples and calibration gases.
- Performed oxidation testing on Grafoil material in support of fission product inventory analysis for AGR-3/4
- Completed pre-burn leaching of all 40 AGR-5/6/7 compacts with 40%-packing fraction for confirmatory LBL analysis. Post-burn leaching of first 20 compacts and burn of second 20 compacts are in progress.
- Received shipping drums back from ORNL at the Hot Fuel Examination Facility (HFEF) at INL.
- Transferred samples (from AGR-3/4 compact radial deconsolidations, AGR-3/4 irradiation capsule components, and AGR-2 compact holders) out of Hot Cell 5 at the Analytical Laboratory to enable continued analyses while the Hot Cell 5 window is replaced.
- Completed fiscal year (FY)-18 work scope for AGR-2 UCO kernel examinations by the University of Florida.
- Paper accepted for publication in *Nuclear Engineering and Design*: T. Lillo, I. J. van Rooyen, J. Aguiar, "Silicon carbide grain boundary distributions, irradiation conditions, and silver retention in irradiated AGR-1 TRISO fuel particles."

December

- Completed a 300-h, 1600°C safety test of AGR-2 UCO Compact 6-2-2 in the ORNL CCCTF.
- Completed six-hour gamma scanning with the IMGA of 30 particles from as-irradiated AGR-2 Compact 5-4-2. These will be subjected to loose-particle safety testing in the FITT.
- Completed burn-leach of the graphite holder from the second safety-tested compact containing PBMR particles (Compact 4-2-1). Leachate solutions are being analyzed.

- Completed burn-leach of particles from safety-tested PBMR Compact 4-3-1, and leachate solutions are being analyzed.
- Completed burn-leach of matrix from as-irradiated PBMR Compact 4-3-2. Leachate solutions are being analyzed.
- Initiated gamma scanning with IMGA of particles deconsolidated from UCO Compact 6-2-3.
- Materialography of particles from 1700°C safety-tested AGR-2 UO_2 Compact 3-4-1 is in progress.
- Initiated x-ray tomography of particles selected from as-irradiated AGR-2 UCO Compact 2-2-1.
- Completed development of mounting procedure and impact parameter optimization using the hot-cell fixture for impact-cracking particles for re-irradiation and safety testing.
- Selected and packaged four AGR-2 Compacts for shipment from INL to ORNL in early January 2018 from Compacts:
  - 6-4-3 (for 1800°C safety testing)
  - 2-4-2, 2-4-1, and 2-3-3 (for temperature transient testing, probably in FY-19).
- Mounted surrogate TRISO particles and ground to near mid-plane in preparation for AGR-2 loose particle ceramography on particles from AGR-2 Compacts 3-3-1, 5-3-3, 5-4-2, and 6-3-3. Initial observations of the surrogate particles were made on the microscope to judge proximity to mid-plane, and now the final polishing is underway.
- Mounted un-irradiated AGR-3/4 compacts, sectioned above the center, and ground to near the centerline. Initial observations were made on the microscope to judge proximity to the centerline, and now the final polishing is underway. This is in preparation for ceramography of three irradiated AGR-3/4 compacts (5-2, 7-2, and 12-2) to observe the morphology of designed-to-fail (DTF) particles.
- Transferred 150 radial deconsolidated particles from AGR-3/4 Compact 3-3 from the Analytical Laboratory to HFEF for gamma counting in the out-of-cell gamma (HOG) station. Twenty-four (24) of these particles have been transferred to the HOG and gamma counting initiated.
- Completed 1400°C heating test of AGR-3/4 Compact 10-4. Post-cleanup run will be completed in January.
- Completed leaching of the condensate plates from AGR-3/4 Compact 3-2 heating test and AGR-2 Compact 6-4-1 re-irradiation safety test in the Analytical Laboratory. Solutions are ready for gamma counting and Sr analysis.
- Made initial entry at Cell 5 at the Analytical Laboratory in order to begin hot cell window replacement.
- Completed the design package for the out-of-cell equipment for the AMIX furnace. The final design review for the out-of-cell equipment will run from January 8 through January 22.
- Completed ~65% of the planned test matrix for high-temperature steam oxidation of graphitic matrix material. Also completed fabrication and characterization of 200 additional matrix specimens to provide sufficient material to complete the high-temperature steam-oxidation study and initiate the low-temperature kinetic-regime oxidation study.
- Completed post-burn leaching of all 40 AGR-5/6/7 compacts with 40%-packing fraction for confirmatory LBL analysis.
- Completed deconsolidation, pre-burn leaching, and burn of first 20 AGR-5/6/7 compacts with 25%-packing fraction and post-burn leaching is in progress.

- Held Technical Coordination Team video conference on December 6. Presentations given by INL included:
  - AGR-3/4 Phase II post-irradiation examination (PIE) plan
  - Summary of AGR-3/4 PIE progress since May 2017
  - Comparison of destructive fission-product measurements versus gamma tomography versus model predictions
  - Update on the development of the air/moisture ingress furnace
  - Discussions of a preliminary air/moisture heating test matrix.

1.2 High-temperature Materials Development

Highlights of high-temperature materials activities during October through December 2017 are as follows:

October

- Started two short to intermediate-term Alloy 617 U-notched weld metal-creep rupture tests.
- Three base metal Alloy 617 U-notched tests are currently ongoing.
- Balloted time-dependent allowable stresses and extension of physical properties in Section III Subgroup Materials, Fabrication and Evaluation and Section II subgroup Non Ferrous Alloys. Addressed comments; there were no negative ballots.
- Staff from INL participated in American Society of Mechanical Engineers (ASME) Code Week, in Phoenix, AZ, October 29–November 1, 2017.

November

- Balloted time-dependent allowable stresses and extension of physical properties in Section III Subgroup Materials, Fabrication and Evaluation and Section II subgroup Non Ferrous Alloys and Subgroup Physical Properties. Comments were addressed and the ballots passed.
- Completed 1000°C, 20 MPa creep test for base metal large-radius U-notch specimen. Two small-radius U-notch tests are ongoing (750°C, 145 MPa and 1000°C, 20 MPa).
- A long term V-notch test was started at 800°C, 35 MPa, with expected life of 100,000 hours.
- Two short-term weld metal U-notch specimens (one small and one large radius) are ongoing (800°C, 110 MPa).

December

- Balloted time-dependent allowable stresses and extension of physical properties in Section III Subgroup Materials, Fabrication and Evaluation and Section II subgroup Non-Ferrous Alloys and Subgroup Physical Properties. Comments were addressed and the ballots passed. The next ballots for these items will be at the Section II committee level.
- Design fatigue curves (ASME Item 16-1000) are being balloted in Subgroup Design Methods.
- A long term V-notch test at conditions of 800°C and 35 MPa with an expected rupture life of 100,000 hours is ongoing. It has currently completed ~850 hours of testing.
- The two short-term Alloy 617 U-notched (one small and one large radius) weld metal creep rupture tests are still ongoing, with conditions at 800°C and 110 MPa and current test duration of ~800 hours for both tests.

- Testing is being performed on two different radii Bridgman notch specimens, small and large radius specimen types.

1.3 Graphite Development and Qualification

Highlights of graphite development and qualification activities during October through December 2017 are as follows:

October

- Drafted the advanced graphite creep (AGC)-3 Specimen Post-Irradiation Data Package Report, with completion pending review and editing.
- *Carbon* manuscript "Beyond the Classical Kinetic Model for Chronic Graphite Oxidation by Moisture in High Temperature Gas-Cooled Reactors" by C. I. Contescu, R. W. Mee, Y. Lee, J. D. Arregui-Mena, N. C. Gallego, T. D. Burchell, J. J. Kane and W. E. Windes has been accepted for publication.
- Continued investigation of gas adsorption (N_2, Ar and Kr) on nuclear graphite, aimed at obtaining information on the amount of energetically uniform surface sites on basal planes and energetically heterogeneous sites at edge and surface defects.
- Machined new graphite samples with lower thickness for repeating the measurements because results on water permeability through four grades of graphite received from Porous Materials Inc., in Ithaca, NY, show that fine-grain materials (IG-110 and 2114) have very low permeability.
- Attended the ASME Boiler Code week (October 30–November 2, 2017). The general graphite code is complete, but small (and significant) changes are occurring resulting from nomenclature changes to the overall code in the new Division 5, Section III.
- Will initiate activity to fill out ASME graphite material data sheets to act as the primary mechanism for transferring critical material-property values necessary to meet the minimum requirements specified in the ASME Code for graphite components. As no new graphite core vendors have actually used these new material data sheets for their design, the graphite working group has requested that the Department of Energy (DOE) ART graphite program attempt to complete the data sheets utilizing the data generated from the unirradiated Baseline Program.
- Leading the graphite and composite ASME/Nuclear Regulatory Committee (NRC) Roadmap task group, formed upon NRC request for metal, composite, and graphite experts and pertinent NRC staff to identify potential gaps between the ASME Code and NRC licensing requirements for the new high-temperature reactor designs. *NGNP High Temperature Materials White Paper*, INL/EXT-09-17187, Revision 1, identifies materials-related deficiencies and issues will be used as a starting point in this analysis, which will continue through 2018.
- Adjusting temperature-control gas flows and mixtures in the AGC-4 Experiment to bring the capsule temperature to a uniform 800°C across the entire specimen volume. The extended outage for AGC-4 capsule has resulted in a different temperature response than was experienced in the first two irradiation cycles of AGC-4 test train. The changes to the capsule have necessitated modifying the gas flow specifications to higher levels in order to provide more insulating or conducting gases into the five active heat zones of AGC-4. Currently, these modifications have allowed the AGC Experiment engineers to bring zones 1, 2, 4, and 5 within temperature specification (~800°C). However, the center region (Zone 3) is operating at a uniform, but higher than specified 865°C temperature.

November

- Published paper: C I Contescu, R W Mee, Y Lee, J D Arregui-Mena, N C Gallego, T D Burchell, J Kane, W E Windes, "Beyond the classical kinetic model for chronic graphite oxidation by moisture in high temperature gas-cooled reactors", *Carbon* 127 (2018), 158-169.
- Completed measurements on water permeability through four graphite grades and obtained raw data for calculation of water effective diffusivity.
- Identified irradiated graphite specimens and un-irradiated graphite companion specimens for oxidation testing. All specimens are of the NBG-25 grade. Irradiation temperature and dose are between 628 and 680°C and between 6.2 and 6.8 dpa. The plan is to oxidize three specimens each in a thermogravimetric analysis (TGA) at isothermal test temperatures of 620, 650, and 680°C. Additional un-irradiated NBG-25 specimens will confirm performance of button specimens with and without the axial hole (present in the irradiated buttons), and correlate performance of the unirradiated NBG-25 graphite in the TGA to the vertical furnace.
- Developed a test matrix for the Baseline program. This matrix will complete 1 billet of 2114 and 1 billet of IG-110 for comparison to previously analyzed billets of each. Billet to billet variations in the two fine-grain graphite grades can then be made. Fabrication of specimens for this effort is complete.
- Continued irradiation of AGC-4.
- Discussed and addressed several ballots and the current status of the graphite design code. The graphite and composites ASME committees met in October. A consolidated version of the composites code has been compiled and submitted for Section III ballot. The code is complete for SiC/SiC composites but is incomplete for C/C, needing several non-mandatory appendices
- Attended and chaired the Technical Meeting on the Status of the International Atomic Energy Agency (IAEA) Knowledge Base on Nuclear Graphite: November 2–3 2017. The purpose was to review and update the content of the Knowledge Base. The agenda included revision and approval of the working arrangement, membership commitments and contributions, status and plans for the IAEA Nuclear Graphite Knowledge Base Portal, update on country activities related to graphite and data to be submitted to the Knowledge Base, status of the Graphite Oxidation TECDOC and planning for future International Nuclear Graphite Specialist Meetings. The Knowledge Base data archive is currently supporting a coordinated research project on irradiation creep in nuclear graphite along with a number of individual Member State research and reactor-life-extension activities.
- Completed AGC-3 PIE Data Package Report, which summarizes non-destructive material-property testing results for all AGC-3 graphite samples (Level 2 milestone: M2NT-18IN060504031). Trends in the data from these tests will be analyzed in a future AGC-3 Data Analysis report.

December

- Conducted the first tensile testing of a billet of grade 2114 graphite at ORNL. A total of 21 specimens were tested and these preliminary data transmitted to INL.
- Submitted a draft report for x-ray diffraction (XRD) and SANS work on highly oriented pyrolytic graphite and selected AGC-1 graphite samples to INL for review. The report fulfills the milestone on the ORNL FY-17 memorandum purchase order.
- Issued the ART Level 2 Milestone (M2NT-18IN060504031), "Complete AGC-3 Post-Irradiation Examination Data Package," December 5, 2017.

1.4 Methods

Highlights of Methods activities during October through December 2017 are as follows:

October

- Received the University of Michigan results for Exercise 3 of Organization for Economic Cooperation and Development (OECD)/ Nuclear Energy Agency (NEA) modular high-temperature gas-cooled reactor (MHTGR)-350 benchmark Phase I. The combined set of participant data submitted for Phases I and III is currently being analyzed and will be issued to the OECD and DOE as two reports in January 2018.
- Received new silicon controlled rectifier for initial benchtop testing of new heater-rod configuration for the High Temperature Test Facility (HTTF) at Oregon State University.

November

- Continued processing results received for Phases I and II of the OECD/NEA MHTGR-350 benchmark. The combined set of participant data will be issued to the OECD and DOE in January 2018.
- Created a set of 1,000 perturbed cross sections with Standardized Computer Analyses for Licensing Evaluation (SCALE)/SAMPLER to be used in the PHISICS/RELAP5-3D core model, as part of the IAEA Coordinated Research Project (CRP) on high-temperature gas-cooled reactor (HTGR) uncertainties. The first set of 1,000 neutronics-only steady states will be created in December and January and will form the basis for the Phase II benchmark specifications.
- Received the redesigned HTTF heater rods and began benchtop testing of them. Initial measurements showed good functionality, but higher than desired electrical resistance.

December

- Issued a level 3 milestone comparison report on the results obtained for Phases I and III of the OECD/NEA MHTGR-350 benchmark (December 22, 2018).
- Continued benchtop testing of the new HTTF heater rods.
- Issued test acceptance reports for the rest of the HTTF tests that have been completed.

2. SIGNIFICANT ACCOMPLISHMENTS

2.1 Fuels Development

2.1.1 Safety Testing and Post Irradiation Examination

In each AGR-3/4 irradiation capsule, four compacts were stacked in the center of a hollow cylinder (inner ring) of nuclear graphite or graphitic matrix material (depending on the capsule). This inner ring was nested within an outer ring of nuclear graphite. Fission products escaping the compacts migrate radially outward to the inner ring and then to the outer ring. The goal of the experiment was to enable measurements of fission-product transport parameters (i.e., diffusion coefficients) in graphite and graphitic materials. In support of this goal, physical sampling has been employed as part of an effort to measure the radial fission-product concentration within the inner and outer rings. To date, inner and outer rings from Capsules 3, 5, 7, and 8 have been sampled, and fission-product analyses are in-progress.

Physical sampling of AGR-3/4 rings involves the use of an end-mill to radially remove material from the rings, a cyclone separator to collect that material, and a series of methods to analyze the fission-product content in the collected material. Depending on the ring, eight to twelve samples were obtained across the wall thickness of the ring (from the outside to the inside surface of the ring). Most rings were

sampled at two axial locations: top or bottom and center. This ring material was sent to Pacific Northwest National Laboratory for fission-product analysis. Preliminary results for the top and center of the Capsule 7 inner ring (IR-07) are given below.

Figure 1 shows the radial fission-product concentrations across the ring wall thickness for IR-07. The samples were taken from a 10 mm tall section at the axial top of the ring. Figure 2 shows the radial fission-product concentrations across IR-07 from a 10 mm tall section at the axial center of the ring. The measured activities from each sample were decay-corrected to the end-of-irradiation plus one day. To give fission-product concentrations, these activities were then divided by the volume of the ring material removed from the ring for each sample. Currently there are some data points missing from the plots because not all of the data from IR-07 have been received. From the top of IR-07 (Figure 1), scans of two middle segments and the radially outermost segment (IR-07 Top outer surface) are not yet available. From the axial center of IR-07 (Figure 2), scans of the two innermost segments, the outermost segment, and one middle segment are not yet available. Note that the Eu-154 profiles are peaked near the inner surface of the ring, but are relatively flat across the thickness of the ring. This could indicate that Eu-154 from the compacts is primarily deposited on the inner surface of the ring (sorption-limited transport), but that it does not diffuse rapidly through the graphitic matrix material of IR-07. In-contrast, the Ag-110m concentration is not appreciably peaked at the inner or outer surfaces. The linear profiles for Cs-134/137 indicate that Fickian diffusion is the dominant transport mechanism for Cs through the rings. Furthermore, comparing these measured fission-product concentrations to those derived from non-destructive gamma-emission computed tomography (GECT) (Humrickhouse 2016), it appears that a peaked concentration at the radial center of the ring wall is an artifact of the GECT data processing.

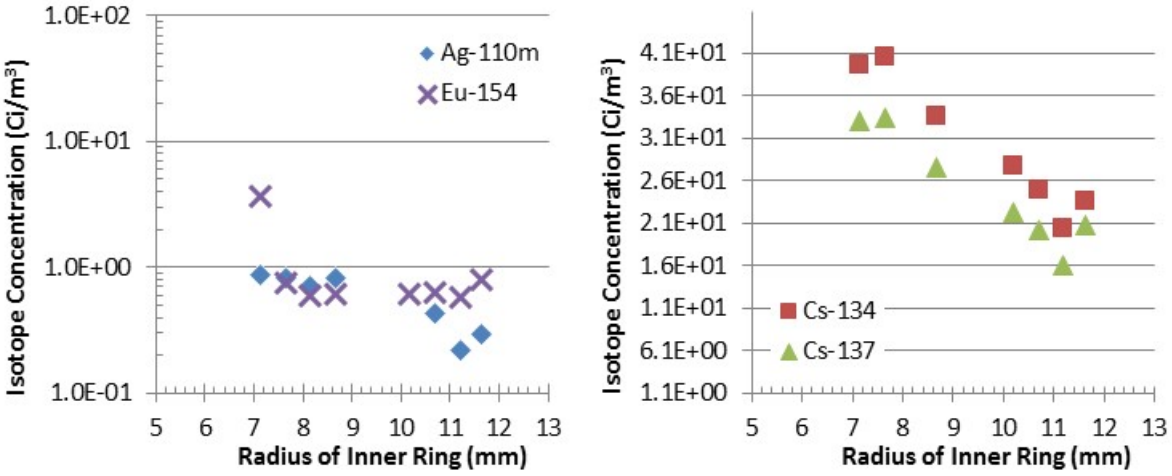

Figure 1. Radial fission-product concentration profiles from the upper most 10 mm of IR-07. Radial concentration of Eu-154 and Ag-110m (left), and radial concentrations of Cs-134/137 (right).

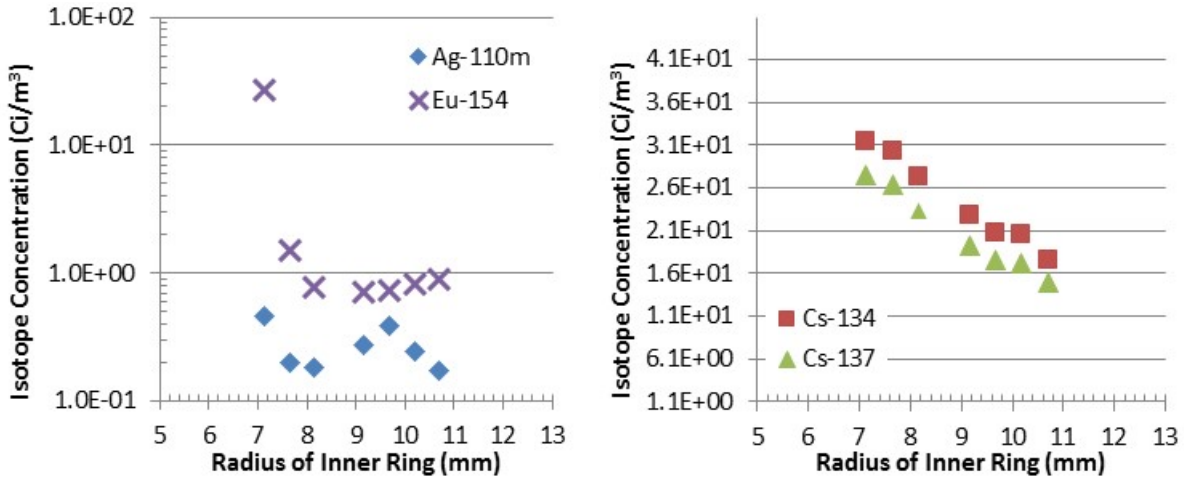

Figure 2. Radial fission-product concentration profiles from a 10 mm section at the axial center of IR-07. Radial concentration of Eu-154 and Ag-110m (left), and radial concentrations of Cs-134/137 (right).

References

Humrickhouse, P. W. et al., (2016), "Modeling and Analysis of Fission Product Transport in the AGR-3/4 Experiment," *Proceedings of HTR2016 Las Vegas Nevada, USA, November 6-10*.

2.1.1.1 1400°C Heating Test of AGR-3/4 Compact 10-4

AGR-3/4 Compact 10-4 was heated at 1400°C for 300 hours in the FACS furnace at INL. The FACS furnace features a water-cooled cold finger with a condensation plate on its end. This plate acts as a cool surface to collect condensable fission products released from the compact. Condensation plates are exchanged at various points during the test. The FGMS collects and quantifies any fission gas Kr-85 released during the test. The plan for this test was outlined in PLN-5518, "Test Plan for the 1400°C Heating Test of AGR-3/4 Compact 10-4," including pre-test FACS furnace and FGMS preparations, temperature program, condensation-plate exchanges, and post-test furnace cleanup runs (Stempien 2017). Fabrication parameters and elements of the AGR-3/4 Compact 10-4 irradiation history are given in Table 1. It was estimated that between 9 and 19 failed DTF particles may be present in Compact 10-4 after irradiation and prior to the heating test (Scates 2015).

Table 1. Selected fuel-fabrication and irradiation properties for Compact 10-4.

Compact[a]	10-4
Fuel Compact Fabrication ID[b]	(LEU03-10T-OP2/LEU03-07DTF-OP1)-Z140
Compact Average Burnup (%FIMA)[c]	11.43
Compact average Fast Fluence (n/m^2, E > 0.18 MeV)[c]	3.75×10^{25}
TAVA Irradiation Temperature (°C)[d]	1168
TA Peak Irradiation Temperature (°C)[e]	1231
TA Minimum Irradiation Temperature (°C)[e]	1079

a. X-Y naming convention denotes location in irradiation test train: Capsule-Level (Demkowicz 2017).
b. From (Collin 2011) and (Hunn, Trammel, and Montgomery, 2011).
c. Based on physics calculations (Sterbentz 2015).
d. TAVA = Time-average volume average temperature determined from thermal calculations (Hawkes 2016).
e. TA = Time-average temperature, determined from thermal calculations (Hawkes 2016).

After completion of the heating test, each condensation plate was gamma counted at the HOG station. In total, 22 plates were used during the test. The measured gamma activities on each plate were decay corrected back to the end of the AGR-3/4 irradiation plus one day (EOI+1). The AGR-3/4 irradiation ended on April 12, 2014, at 5:00 AM MT. The decay-corrected activities were then divided by pre-determined condensation-plate collection efficiencies measured at 1600°C in the FACS furnace. In the future, collection efficiencies at 1400°C could be measured, and the data adjusted accordingly. To give the measured compact fraction released from the fuel, the decay-corrected and efficiency-corrected activities are then divided by the predicted compact fission-product inventory from physics calculations in (Sterbentz 2015). Figure 3 summarizes the cumulative compact fraction of fission products released as a function of the time from the moment the furnace started to heat. The dashed line labeled "Particle" is the compact-inventory equivalent to a single particle. Releases less than this dashed line are less than a particle inventory of fission products. The FACS furnace temperature measured at the thermocouple in the sample holder is plotted on the right vertical axis.

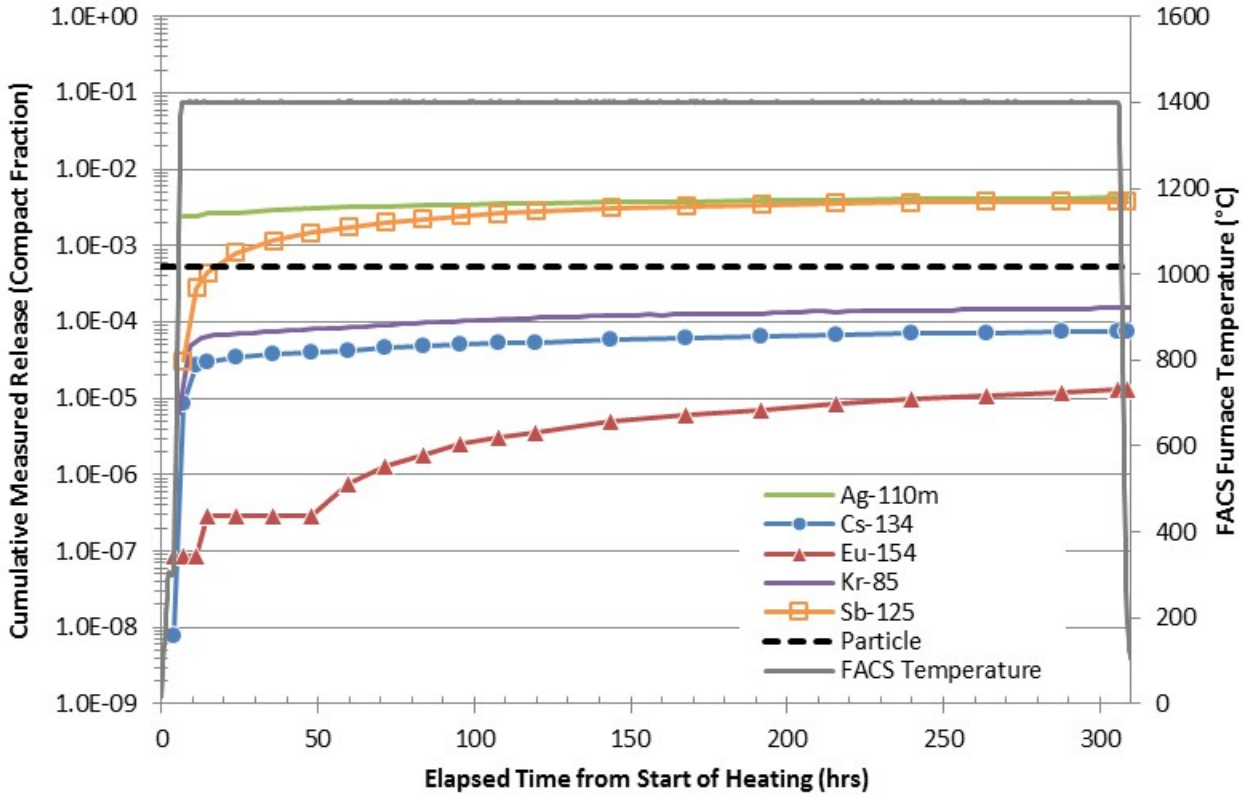

Figure 3. Total compact fractions of fission products measured from condensation plates from the heating test of Compact 10-4. FACS furnace temperature is also plotted along with the compact fraction equivalent to one particle inventory (5.29E-4).

Figure 3 shows that the majority of transportable Ag-110m was released early on in the test and during the ramp to 1400°C. The total fraction of Sb-125 released by the end of the test is similar to that of Ag-110m; however, the Sb-125 release occurred over a longer period of time, and the rate of the Sb-125 release decreased steadily throughout the test. The first few condensation plates contained the majority of the Cs-134, and the rate of Cs-134 release decreased as the test progressed. Compact 10-4 had 20 DTF particles (with no SiC layer), and it was expected that the majority of the Cs from these particles would be released in-pile during irradiation in Advanced Test Reactor (ATR). Only 14% of a single particle inventory of Cs-134 was measured on the condensation plates, supporting the expectation that the DTF particles would release Cs-134 in-pile. Europium-154 releases were gradual and well below the inventory

of a single particle. Note that only two of the first seven condensation plates had measurable Eu-154, giving the stepped appearance of the Eu-154 data prior to 50 hours. Finally, the majority of the measured Kr-85 was released early in the test and amounted to 29% of a single particle inventory. This indicates that the majority of Kr-85 from failed DTF particles was released in-pile and that any DTF particles that might have remained intact after irradiation (and prior to the heating test) did not substantially contribute additional Kr-85.

References

Demkowicz, Paul A., 2017, "AGR-3/4 Phase 2 Post-Irradiation Examination Plan," PLN-5382, Idaho National Laboratory, May 5, 2017.

Hawkes, Grant L., 2016, "AGR-3/4 Daily As-Run Thermal Analyses," ECAR-2807, Rev. 1, Idaho National Laboratory, April 21, 2016.

Hunn, J., M.P. Trammell, and F.C. Montgomery, 2011, *Data Compilation for AGR-3/4 Designed-to-Fail (DTF) Fuel Compact Lot (LEU03-10TOP2/LEU03-07DTF-OP1)-Z*, ORNL/TM-2011/124, Oak Ridge National Laboratory.

Scates, D. M., "Release-to-Birth Ratios for AGR-3/4 Operating Cycles 151A through 155B", ECAR-2457, Rev. 1, June 5, 2015.

Stempien, J. D., 2017e, "Test Plan for the 1400°C Heating Test of AGR-3/4 Compact 10-4", PLN-5518, Idaho National Laboratory, November 2017.

Sterbentz, James W., 2015, "JMOCUP As-Run Daily Physics Depletion Calculation for the AGR-3/4 TRISO Particle Experiment in the ATR Northeast Flux Trap," ECAR-2753, Rev. 1, Idaho National Laboratory, September 2015.

2.1.2 Safety Testing and Post-irradiation Examination at ORNL

2.1.2.1 High Temperature Steam Oxidation of AGR-5/6/7 Matrix Material

Introduction

Accident scenarios for HTGR include air- and moisture-ingress events that occur at elevated temperatures. The HTGR fuel system consists of TRISO coated fuel particles compacted into a matrix of graphite and carbonized resin. To understand overall fuel performance under accident conditions, the oxidation behavior of each component must be understood. Separate effects tests are currently being carried out on matrix material, rather than integral tests on compacts containing TRISO particles, to isolate the oxidation behavior of the matrix material and allow for the determination of matrix material oxidation rates. Empirical oxidation rates for the matrix material are required to build complex fuel-performance models which can be used to accurately simulate integral fuel systems in a variety of fuel configurations and environments.

Moisture-ingress scenarios may be initiated by breaking one or more tubes in a steam generator where steam leaks into the primary system and the primary system may slowly depressurize over the course of hours. The various scenarios lead to a range of oxidation environments, with possible fuel temperatures ranging from 1000–1600°C and steam partial pressures (pH_2O) ≤2 kPa for tens of hours or ≤400 kPa for up to several hours, depending on the accident scenario.

Limited insight is present in the literature concerning steam oxidation of the carbonaceous matrix. Experiments on the oxidation behavior of matrix materials in air at relevant operational temperatures have been conducted (Contescu et al. 2008, Lee et al. 2014), but limited exploration of the impact of steam on oxidation performance of matrix materials exists. Steam oxidation testing of nuclear-grade graphite has been reported but is generally limited to the kinetic regime (T <1100°C, pH_2O 0.01–3 kPa) (Contescu et

al. 2014, Overholser and Blakely 1965). It is plausible that accident conditions will exceed these test conditions; thus, elevated temperatures at higher steam partial pressures must be explored.

The initial focus of planned separate-effects testing is to empirically determine the oxidation rate of matrix material in a steam environment at high temperatures relevant to HTGR accident scenarios. This will provide insight on the oxidation performance of matrix similar to that present in the AGR-5/6/7 fuel. Because of the limited understanding of the performance of matrix material in steam at high temperatures, the test conditions will be modified as the experiment progresses to explore the variables impacting oxidation performance. Disc-shaped matrix samples have been produced for steam -xidation testing and high-temperature steam-oxidation testing is currently underway.

Preparation of Matrix-only Test Samples

The graphite and resin blend used to produce matrix samples for separate-effects testing was obtained from BWX Technologies and was equivalent to that used to produce AGR-5/6/7 compacts. The targeted sample geometry for the test samples was selected to limit density variation across the thickness of the specimen and maintain a surface-area-to-volume ratio of approximately 1:1 to minimize volume effects during oxidation testing (Contescu et al. 2008). The selected disc geometry was 12.1-mm diameter and 2.6-mm thick. The samples were produced to meet the AGR-5/6/7 fuel specification for matrix density, with the primary criterion being a density $\geq$1.65 g/cm^3 while targeting a density of 1.75 g/cm^3. Matrix samples were produced in a multi-step process. The production route consisted of preparing a sample charge, pressing a green compact, carbonizing samples, and heat treating those samples in a final step to drive out impurities. The sample ID was tracked throughout the production process, and measurements were taken at interim stages such that possible variations in sample properties and initial density could be tracked and understood.

The matrix-only samples are expected to have a similar chemical composition, but a different microstructure compared to the AGR-5/6/7 fuel compacts. The absence of fuel particles in the matrix-only samples will impact the overall orientation of the graphite flake and the local variation in matrix density. In addition, while carbonization and heat treatment conditions were the same for the matrix samples and the fuel compacts, the equipment used was different, and the pressing procedure to make the matrix-only samples was optimized for the equipment and the geometry of the oxidation test samples. Microstructural differences could impact oxidation behavior and should be accounted for in the final analysis of the results. Some comparative analysis of the microstructure in the matrix-only disc versus AGR-5/6/7 fuel compacts is planned.

Pressing was initiated by first weighing 0.6200 g of the graphite/resin blend and hand-pressing the material to produce a die charge. This charge was then lightly-ground with SiC-grit sanding paper to achieve a sample with a mass of approximately 0.5800 g. This step was implemented to achieve samples with consistent mass. A green compact was produced by hot pressing the charge in a die heated at 155°C and subjecting it to 1.3 kN for 60 s using the Promess automated servo-driven mechanical press shown in Figure 4.

Figure 4. Promess automated servo press.

The green compacts were then subjected to a carbonization step to finish curing and carbonize the resin binder. This thermal exposure was done in a Lindberg/Blue tube furnace. The carbonization schedule is shown in Table 2 and follows the same temperature profile as those used to produce fuel compacts.

Table 2. Carbonization schedule for matrix samples.

Step	Ramp Rate	Step Duration
20°C → 140°C	4.0°C/min	30 min
140°C → 220°C	1.0°C/min	80 min
220°C → 330°C	1.33°C/min	83 min
330°C → 420°C	0.5°C/min	180 min
420°C → 560°C	0.83°C/min	168 min
560°C → 610°C	2.0°C/min	25 min
610°C → 690°C	4.0°C/min	20 min
690°C → 900°C	6.0°C/min	35 min
900°C → 900°C	hold temperature	30 min
900°C → 20°C	20.0°C/min	44 min

After carbonization, the samples were subjected to a final high-temperature heat treatment at 1800°C for one hour (20 C/min ramp from 20 to 1800°C). The heat treatment was performed under vacuum with a starting vacuum of <~100 Pa in a Thermal Technology, Inc., ASTRO furnace. This step drives out impurities present in the sample and yields the final geometry and density. Minimal geometry variation was observed after the high-temperature heat treatment relative to the post-carbonization sample.

Matrix Sample Inspection for Acceptance

The final heat-treated samples were subjected to dimensional inspection and density calculation according to AGR-CHAR-DAM-39, which is a previously developed procedure for matrix-only compact dimension and density measurements from the AGR program. The thin (2.6-mm-thick), disc-shaped matrix samples did not allow for the diameter to be measured at multiple axial positions per the procedure used for one-inch-long compacts; therefore, some modifications to the procedure were instituted. Notably, the diameter measurement was taken at the middle of the sample as opposed to three positions along the

length (near top, middle, and near bottom) used for standard one-inch-long cylindrical compacts. Three unique measurements around the circumference of the sample (~60 degree increments) were taken in lieu of measurements at different axial positions. Measurements of sample dimensions and mass were performed on calibrated equipment and satisfied applicable NQA-1 standards. This included validation of balances and calipers prior to obtaining measurements through the use of certified mass standards and gauge blocks.

Acceptance criteria included the sample density and a visual inspection of the sample surface. The matrix density was required to be ≥1.65 g/cm^3 per the fuel specification. In addition, samples with a density outside two standard deviations of the measured mean were rejected to reduce the sample-to-sample variability. The final criterion for acceptance was a visual inspection. The most common reason for sample rejection after visual inspection was surface irregularities that would increase total surface area. This included cracks and circumferential fissures. The circumferential fissures were expected as they were commonly observed in previous efforts to press larger matrix-only compacts from graphite/resin blends similar to the AGR-5/6/7 composition using similar approaches. Figure 5 shows examples of circumferential fissures in rejected samples.

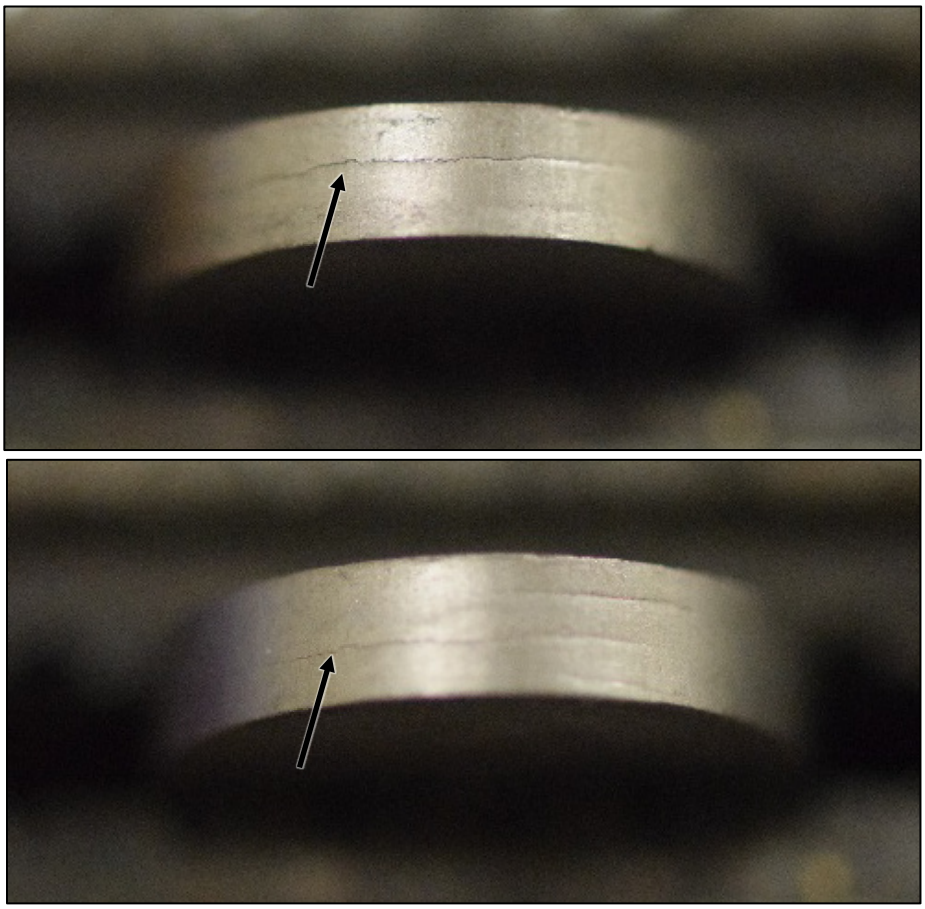

Figure 5. Examples of circumferential fissures in rejected heat-treated matrix samples.

Figure 6 shows the inspection results for the first 150 samples produced. The average density of the final sample set was 1.768 g/cm^3 with a standard deviation of 0.023 g/cm^3. Only six samples had a density more than two standard deviations from the mean. Visual cracking was the primary reason for sample rejection. The final sample yield was 43%. Because of the low yield, a second set of 150 samples is being produced to ensure enough acceptable samples are available to complete the high-temperature steam

oxidation testing. This second set of samples has been pressed and heat treated and is awaiting final density analysis and visual inspection. The second set of samples is also necessary to complete planned steam oxidation testing in the kinetic regime (800–1000°C, 2–1000 Pa pH_2O).

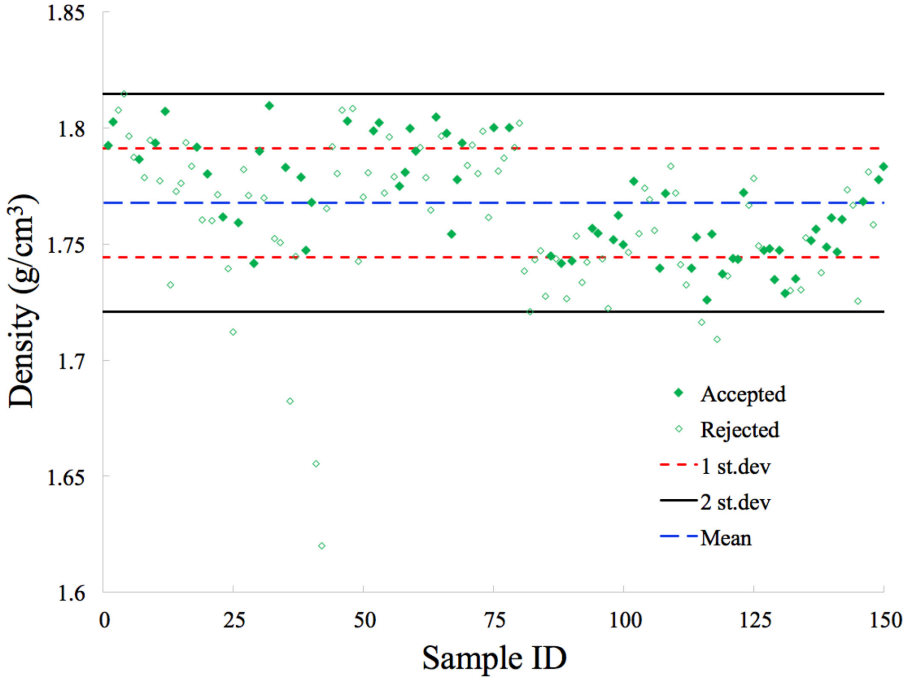

Figure 6. Density after final heat treatment (HT) versus production ID for matrix samples.

Experimental Set-up

The furnace identified for the high temperature steam testing is the High Temperature Furnace Module (HTM) in the ORNL Severe Accident Test Station (SATS). The furnace is capable of operation above 1600°C and up to 100% steam conditions (with a total pressure within the apparatus approximately equal to atmospheric pressure) [Terrani and Silva 2015]. Figure 7 shows the SATS furnace and a schematic of the HTM. A more detailed view of the setup, including the alumina sample holder, is shown in Figure 8. The matrix sample is suspended in the center of the HTM on the end of an alumina rod using a chemically vapor deposited silicon-carbide axle (Figure 8c). A 1.6-mm hole is drilled in the center of the matrix sample to allow for the sample to be suspended in the furnace. Ultra-high-purity (UHP) He is used as a carrier gas to introduce steam into the HTM from the steam generator. The steam generation rate is controlled by the introduction of H_2O from a peristaltic pump. All steam lines are wrapped with heat tape to eliminate risk of condensation in the system. A UHP He flow rate of 0.5 l/min is used for all tests. The end-cap was modified from the original design to prevent back flow of oxygen at the 0.5 l/min flow rates by utilizing a high-temperature compression fitting to prevent leakage into the alumina tube. Tests are started after the sample is loaded and the UHP He sweep gas has purged the system. The system is considered to be purged when the O_2 impurities are measured to be 200–300 ppm in the outlet line. The oxygen sensor is shown in Figure 8a. The furnace is then ramped to the target temperature at 20°C/min. Once the target temperature is reached, the temperature is held constant, and steam is introduced for the soak period. The steam is then turned off, and the furnace is ramped down to room temperature at 20°C/min.

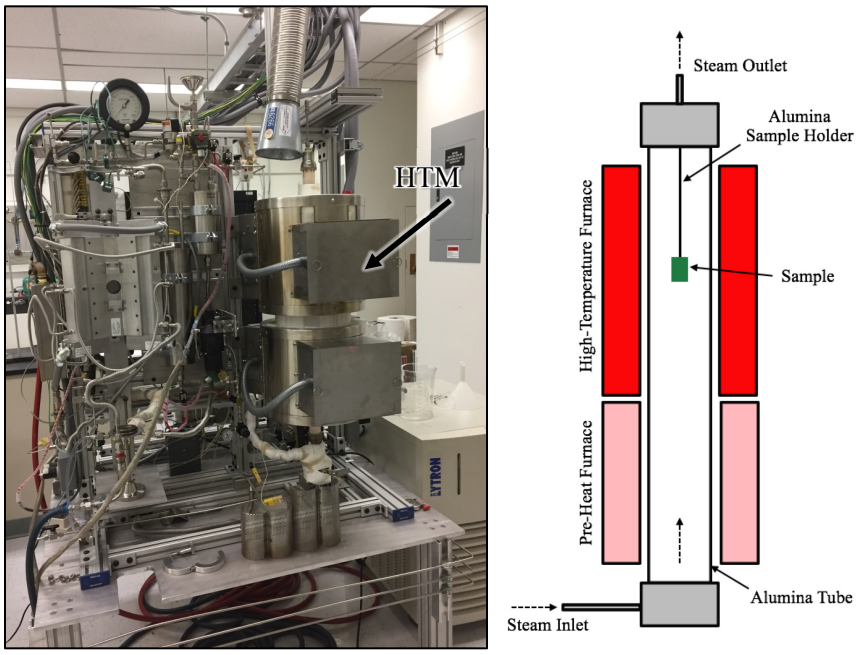

Figure 7. SATS with HTM (left) and schematic of HTM internals (right).

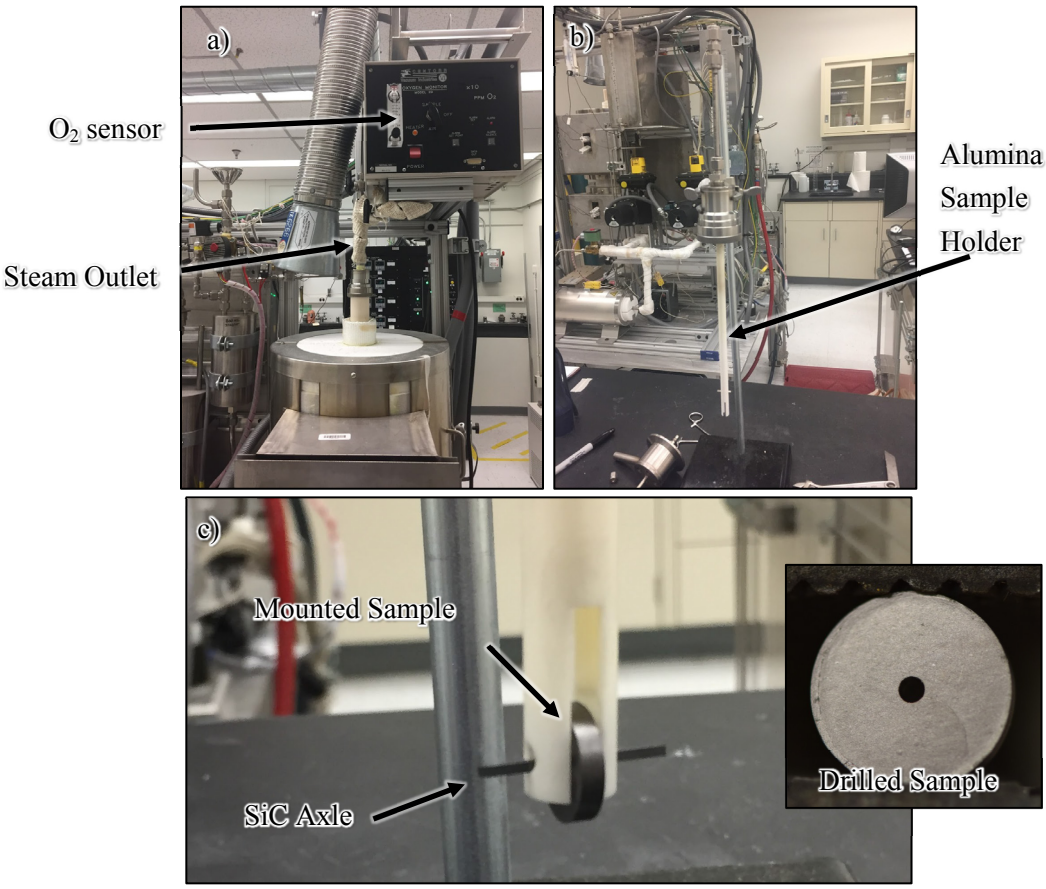

Figure 8. Detailed view of a) HTM furnace top, b) alumina sample holder, and c) sample mounting.

Each sample is conditioned prior to steam oxidation testing after the 1.6 mm hole is drilled in the sample. The conditioning follows the American Society of Testing and Materials standard D7542-09 where the sample is dried in air at 130°C for 3 h then stored immediately in a desiccator. The samples are then weighed to determine their pre-test mass using a calibrated balance which is validated by check weights. The oxidation performance is determined by measuring the total mass loss after exposure. After thermal exposure, the sample is dropped into a pre-weighed aluminum weigh boat to minimize handling and retain all material as the surface of the sample may be friable after steam exposure. The mass of the sample and weigh boat are them measured by the same method as was used for the as-fabricated sample to determine the mass loss.

Results

The initial and revised test matrices for the high-temperature steam oxidation testing are shown in Table 3 and Table 4, respectively. The revised test matrix is responsive to the oxidation results and has been modified as needed. Runs with no steam, only the UHP He carrier gas, are included to determine the extent of oxidation occurring from residual oxygen in the system. The test matrix has also evolved based on initial measurements of oxidations rates. In particular, the oxidation rates at 1400°C provide concern about the survivability of the samples at 1600°C for longer-duration tests. To have a complete data set and explore multiple steam conditions, 1300°C was included.

Table 3. Initial test matrix.

Temperature	Exposure Time*	Approximate Steam Partial Pressure
1200°C	0.5, 1, 4, 6 h	10, 20, 30, 50 kPa
1400°C	0.5, 1, 4, 6 h	10, 20, 30, 50 kPa
1600°C	0.5, 1, 4, 6 h	10, 20, 30, 50 kPa

Table 4. Revised test matrix.

Temperature	Exposure Time*	Approximate Steam Partial Pressure
1200°C	0.25–4 h	0, 1, 10, 20, 50 kPa
1300°C	0.25–2.5 h	0, 1, 10, 20, 50 kPa
1400°C	0.25–2 h	0, 1, 10, 20, 50 kPa
1600°C	0.25–1 h	0, 10 kPa

* At least four time conditions per temperature and pressure combination, depending on feasibility

The initial oxidation results are shown in Figure 9. The mass loss appears to follow a linear trend suggesting that after 0.5-hour exposure, the oxidation rate was constant. The oxidation rate also increased as a function of temperature, as expected. A 0.25-hour run will be conducted for all temperatures of interest to provide insight on the initial oxidation rate for all conditions. Considering the rapid mass loss from samples oxidized at 1400°C with 10 kPa steam, the range of steam pressures for 1600°C testing was reduced, and tests at 1300°C were added. The mass loss associated with residual oxygen was observed to be minimal relative to the mass loss associated with steam oxidation.

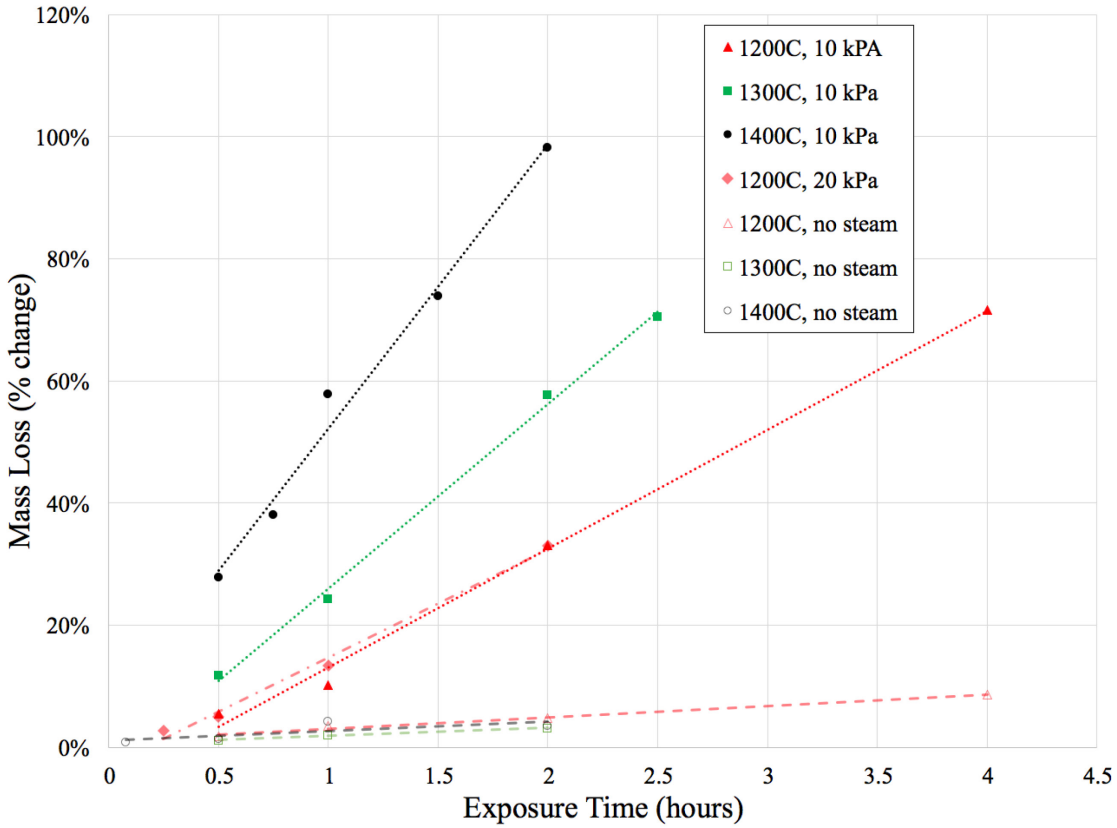

Figure 9. Mass loss as a function of exposure time at 1200°C, 1300°C, and 1400°C, intermediate-dashed lines represent the linear trend line for the no steam tests, the short-dashed lines represent the linear trend line for the 10-kPa tests, and the dot-dash line represents the 20-kPa, 1200°C trend line.

The surface-area-normalized oxidation rates are presented in Figure 10. A primary observation is the apparent saturation of the reaction rate observed with an increase in steam partial pressure between the 1200°C 10 kPa and 20 kPa test conditions. The saturation effect is not unexpected based on the elevated temperatures of the experiment. It is feasible that the experimental conditions represent a mass transfer controlled oxidation regime similar to what is observed for graphite oxidation by oxygen at temperatures above the kinetic regime [Kane et al. 2017]. The observed saturation effect is the primary motivation to include the low pH2O condition of 1 kPa to probe the transition to the mass transfer regime.

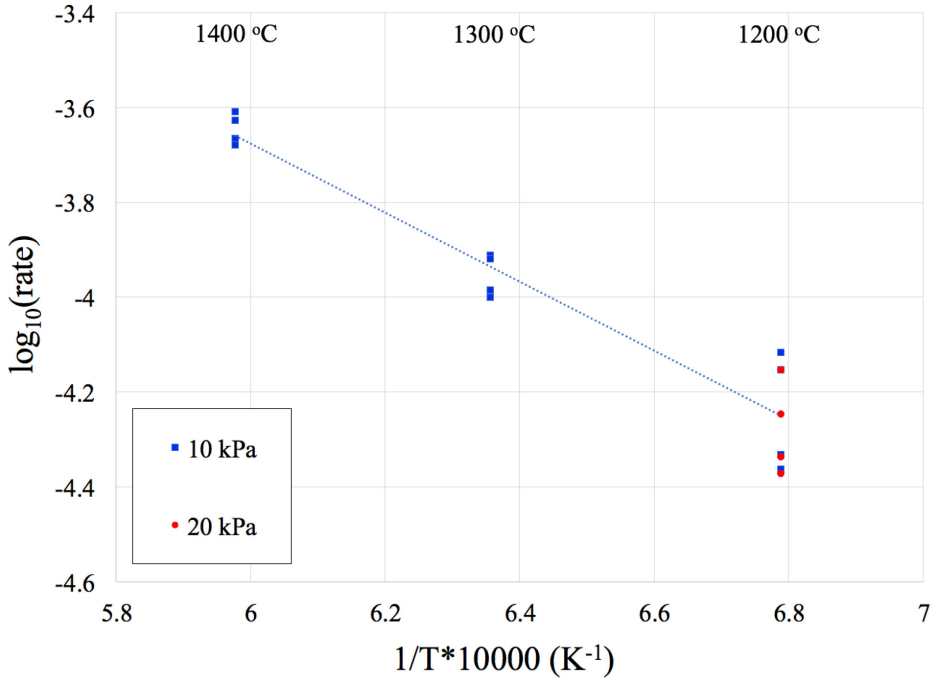

Figure 10. Arrhenius plot of the log of the normalized oxidation rate, r (kg/m^2s) vs. inverse temperature.

Summary

An investigation of oxidation performance of matrix material at high-temperature steam conditions has been undertaken. This effort focused on first producing appropriate matrix samples. Samples met the density criteria defined by the fuel specification and were near the targeted matrix density for compacts. Samples within a range of two standard deviations from the mean were accepted for testing to limit oxidation performance variation based on sample density. Samples were also subjected to an additional acceptance criterion based on the surface appearance of the samples to limit effects from surface irregularities or fissures on the sample surface area. Steam oxidation results showed an expected temperature dependence and suggested a steam-saturation effect. The steam-saturation effect implies the test conditions represent a mass-transfer controlled oxidation regime. Further testing will explore the observed saturation effect and provide potential insight into the steam oxidation mechanism at elevated temperatures and steam partial pressures.

References

Contescu, C.I., S. Azad, D. Miller, M.J. Lance, F.S. Baker, T.D. Burchell, "Practical aspects for characterizing air oxidation of graphite," *Journal of Nuclear Materials* 381.1-2 (2008), 15–24.

Lee, J.J., T.K. Ghosh, S.K. Loyalka, "Oxidation rate of graphitic matrix material in the kinetic regime for VHTR air ingress accident scenarios," Journal of Nuclear Materials 451.1-3 (2014), 48–54.

Contescu, C.I., R.W. Mee, P. Wang, A.V. Romanova, T.D. Burchell, "Oxidation of PCEA nuclear graphite by low water concentrations in helium," Journal of Nuclear Materials 453.1-3 (2014,) 225–232.

Overholser L.G. and J. P. Blakely, "Oxidation of graphite by low concentrations of water vapor and carbon dioxide in helium," Carbon 2.4 (1965), 385–394.

Terrani, K. A. and C. M. Silva (2015). "High temperature steam oxidation of SiC coating layer of TRISO fuel particles." Journal of Nuclear Materials 460: 160-165.

Kane, J. J., C.I. Contescu. R.E. Smith, G. Strydom, W.E. Windes (2017). "Understanding the reaction of nuclear graphite with molecular oxygen: Kinetics, transport, and structural evolution." Journal of Nuclear Materials 493: 343-367.

2.2 High-temperature Materials

2.2.1 ASME Code Activities

2.2.1.1 Alloy 617 Code Case Balloting

The time-dependent allowable stresses and extension of physical properties for Alloy 617 were balloted in Section III Subgroup Materials, Fabrication and Evaluation and Section II subgroup Non-ferrous Alloys and Subgroup Physical Properties. Comments were addressed and both ballots passed. The only substantive comment on the time-dependent allowables was a question about how the effects of very long-term aging were addressed in the background document. In discussion with Section III Working Group on Allowable Stresses, it was determined that the method used in this draft Code Case is consistent with the approach that has been used historically for qualification of Section III Division 5 materials. It was concluded, however, that this issue may warrant further analysis, and a new item number will be established to further consider aging effects on Division 5 materials.

The design fatigue curves for Alloy 617 were approved by voice vote in the working Group on Fatigue Strength at the Phoenix Code Week. These curves were then balloted at the Section III Subgroup level. The proposed curves taken from the Code Case Proposal File are shown below in Figure 11. There was a negative ballot on these curves because of the specification of a strain rate of 4×10^{-3} on the figure. This formulation of the design fatigue curves is consistent with those for all of the materials in Division 5. The effect of slower strain rates, which might be more appropriate for components in service, is likely to be a reduction in the design curves. This effect is not well understood and, for very slow strain rates, is probably not amenable to testing in a reasonable time. While the ballot will likely pass because the conventions used in Division 5 have been followed, this issue will require further consideration within ASME.

Figure HBB-T-1420-1F
Design Fatigue Strain Range, ϵ_t, for Alloy 617

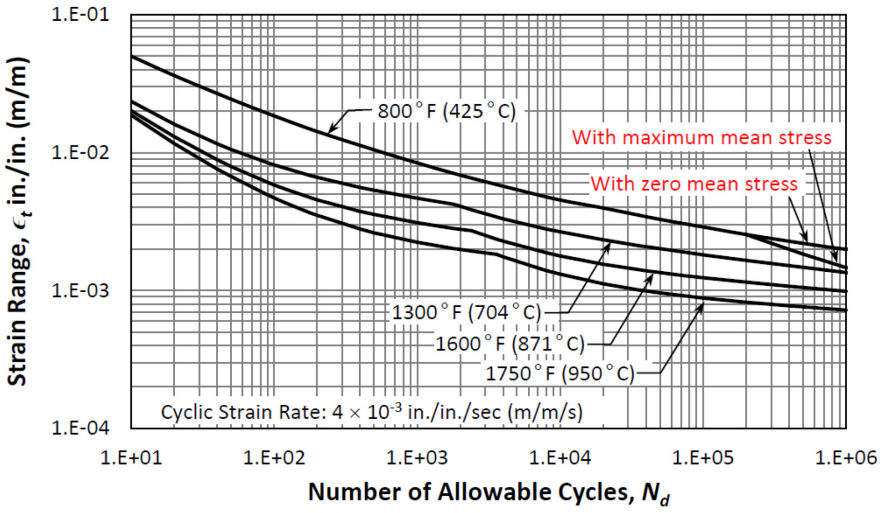

Figure 11. Proposed design fatigue curves for Alloy 617.

2.2.2 Long-term VHTR Materials Qualification

Initial testing is nearly complete for the bridgeman notch (U-notch) specimens. Test conditions ranged from 750 to 1000°C, and stress levels from 145 to 20 MPa. Two types of U-notch specimens have been tested, with large and small radii. All tests have now run to completion for the large radius U-notch specimens. The 750°C, 145 MPa and the 1000°C, 20 MPa tests are still on going for the small radius U-notch specimens. The 800, 900 and 1000°C test conditions were chosen with an expected rupture life of approximate 1200 hours. The 750°C condition has an expected rupture life of approximate 2500 hours. These expected lives are based on creep results of standard straight-gauge specimens. The large radius U-notch specimens, shown in Figure 12a exhibited little change in creep behavior as compared to the straight-gauge tests, with the possible exception of a longer than expected test at 750°C, 145 MPa (the 5800 hour rupture life was over twice the expected life). The small radius U-notch tests (Figure 12b) all extended well beyond the expected rupture life, most particularly the 750°C, 145 MPa condition. As this material, at these conditions, is notch strengthening. It is believed that the small radius of curvature of the notches in these specimens is producing the longer than expected rupture lives (via notch strengthening). Stress states may also play a role. While both notch types create a multiaxial stress state around the notch area, the large radius notches induce a diffuse multiaxial stress state that is close to constant throughout the specimen thickness. The small radius U-notch creates a sharper multiaxial stress state that is larger nearer to the notch tip, and nearly non-existent in the center of the specimen.

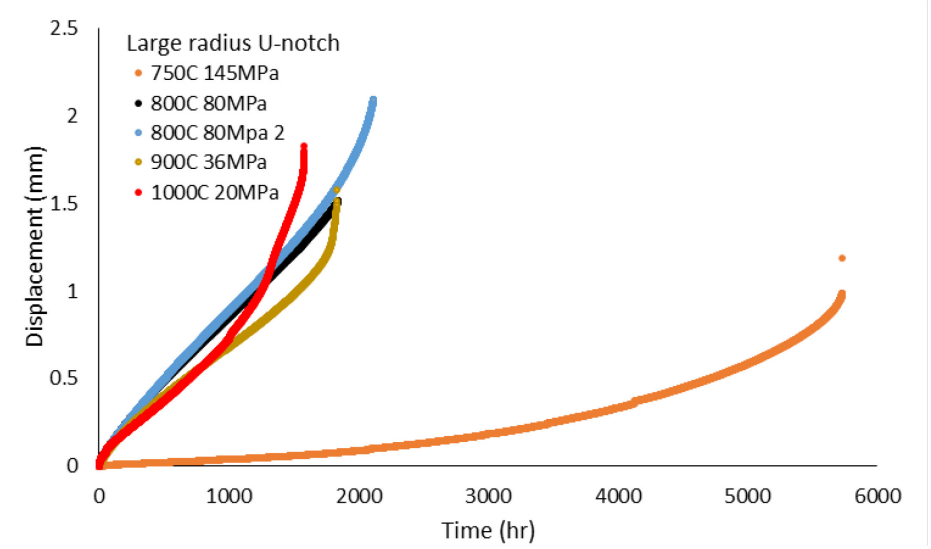

(a)

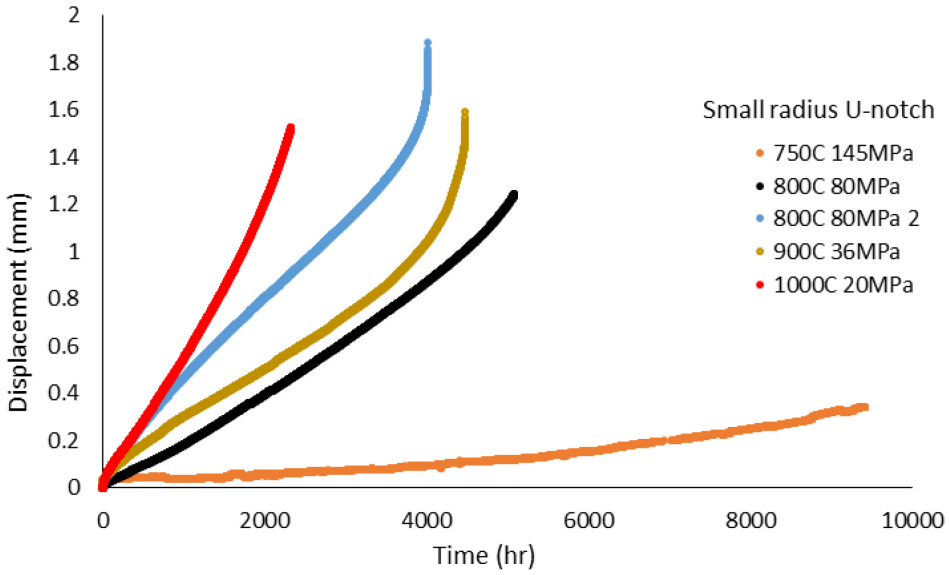

(b)

Figure 12. Creep curves for base metal Bridgeman notch (i.e., U-notch) specimens with (a) large radius and (b) small radius notches.

2.3 Graphite Development and Qualification

2.3.1 Materials—Graphite

2.3.1.1 Tensile Tests

The first ORNL tensile test data for a 2114 billet (Serial No. 116310) have been collected and analyzed. The graphite billet and subsequent first 21 tensile tests were conducted in accordance with the previously delivered and approved experimental plan (ORNL/TM-2016/383). All 21 specimens failed within the gauge section. The tests were conducted at a constant strain rate of 0.00083 in/sec. All specimens were taken from one end section of the ISO-molded billet (see cutting plan in experimental plan). Results are illustrated in Figure 13 and Figure 14 and itemized in Table 5.

The following observations were made:

1. The tensile strength with graing (WG) > against grain (AG) as expected
2. The values of $E_{Initial}$ were always >$E_{Average}$ as expected
3. The E(WG) > E(AG)
4. Edge tensile strength and modulus were >center tensile strength and modulus, as expected.

The measured strengths, although slightly different, as noted above, were significance-tested, and the group means could not be shown to be different. Thus combining all 21 test results gives a mean tensile strength of 29.64 MPa with a standard deviation of 2.44 MPa.

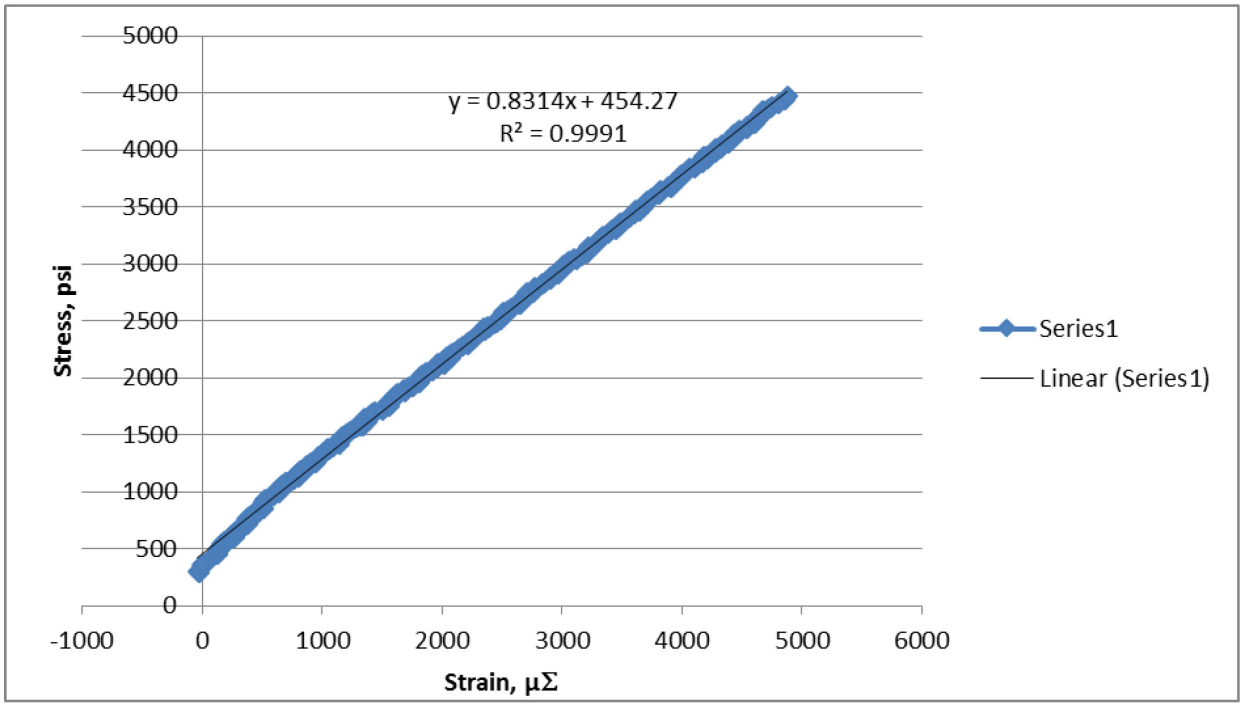

Figure 13. Tensile stress-strain curve for Mercen grade 2114 (billet 116310 specimen 1A1T2L3T). Note the initial modulus is larger than the average modulus.

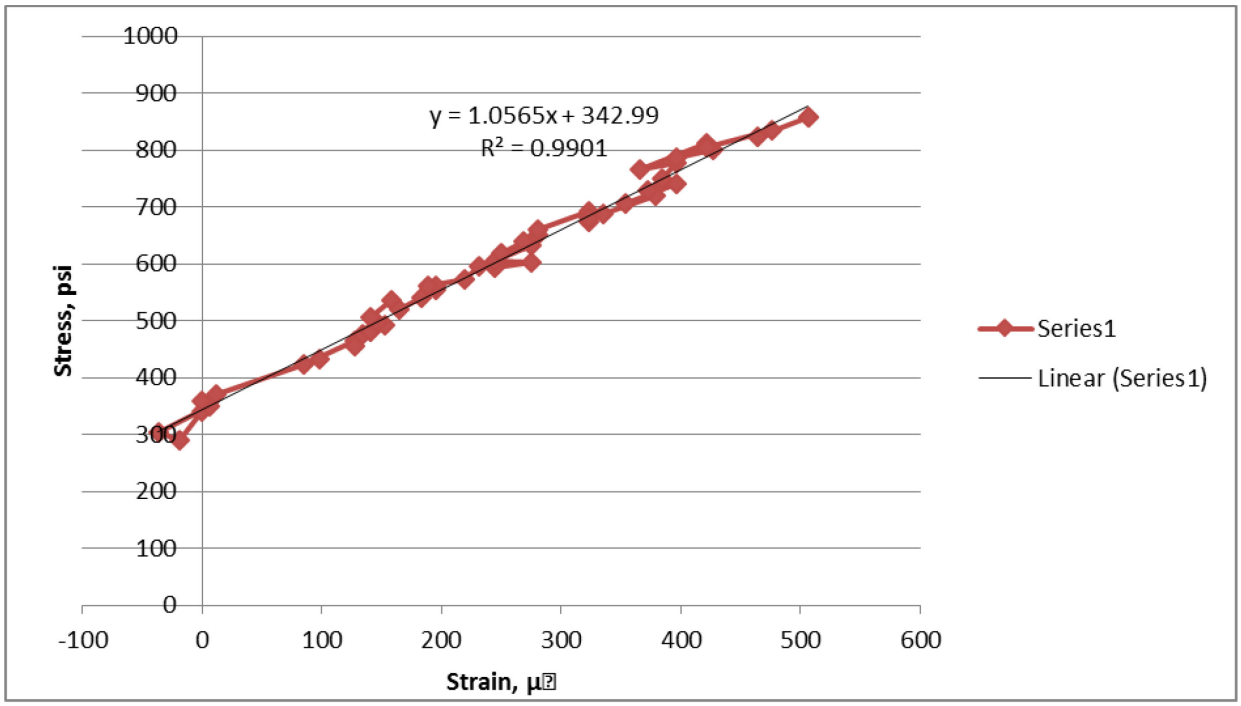

Figure 14. Initial tensile stress-strain curve for Mercen grade 2114 (billet 116310, specimen 1A1T2L3T).

Table 5. Results of initial Grade 2114 (billet 116310) graphite testing.

Specimen Number	Location in billet	Purpose	Gauge Dia	Fracture strength,σ_t		Strain to Failure		Initial Young's Modulus (E)		Ave Young's Modulus	
			(in)	ksi	MPa	με	%	ksi	GPa	ksi	GPa
1A1P1P2T	EDGE (par) (AG)	Billet edge (vs.) Billet center	0.229	3.8252	26.37	4821	0.4821	906.1	6.25	808.5	5.57
1A1P1P4T	EDGE (par) (AG)	Billet edge (vs.) Billet center	0.229	3.7004	25.51	4541	0.4541	942.7	6.50	771.7	5.32
1A1P1P6T	EDGE (par) (AG)	Billet edge (vs.) Billet center	0.229	4.4309	30.55	3839	0.3839	1997	13.77	1082.3	7.46
1B2P1P2T	EDGE (par) (AG)	Billet edge (vs.) Billet center	0.229	4.5287	31.22	5084	0.5084	909	6.27	858.0	5.92
1B2P1P4T	EDGE (par) (AG)	Billet edge (vs.) Billet center	0.229	4.4724	30.84	5090	0.5090	1185.4	8.17	840.8	5.80
1B2P1P6T	EDGE (par) (AG)	Billet edge (vs.) Billet center	0.229	4.3809	30.21	4224	0.4224	1502	10.36	936.0	6.45
		Ave			29.12	4600	0.46		8.55		6.09
		S.D.			2.50	499	0.05		3.01		0.77
1B3P1P2T	CENTER (par) (AG)	Billet edge (vs.) Billet center	0.2295	3.9852	27.48	3186	0.3186	2306	15.90	1136.7	7.84
1B3P4P2T	CENTER (par) (AG)	Billet edge (vs.) Billet center	0.2295	4.2520	29.32	3808	0.3808	2814.2	19.40	1042.9	7.19
1A4P1P2T	CENTRE (par) (AG)	Billet edge (vs.) Billet center	0.2295	4.6910	32.34	4958	0.4958	974.7	6.72	964.4	6.65
1A4P1P4T	CENTRE (par) (AG)	Billet edge (vs.) Billet center	0.229	4.7440	32.71	2954	0.2954	1325	9.14	1.1	0.01
1A4P1P6T	CENTRE (par) (AG)	Billet edge (vs.) Billet center	0.229	4.4728	30.84	3936	0.3936	1623.7	11.20	1632.7	11.26
1B2P4P6T	CENTRE (par) (AG)	Billet edge (vs.) Billet center	0.229	4.0916	28.21	5511	0.5511	976.9	6.74	827.7	5.71
		Ave			30.15	4059	0.41		11.51		6.44
		S.D.			2.16	998	0.10		5.16		3.68
1A1P1P2T	Par, AG oriented spec but crack prop in WG direcion	AG (vs.) WG	0.229	3.8252	26.37	4821	0.4821	906.1	6.25	808.5	5.57
1A1P1P4T	Par, AG	AG (vs.) WG	0.229	3.7004	25.51	4541	0.4541	942.7	6.50	771.7	5.32
1A1P1P6T	Par, AG	AG (vs.) WG	0.229	4.4309	30.55	3839	0.3839	1997	13.77	1082.3	7.46
1A1P4P2T	Par, AG	AG (vs.) WG	0.2295	3.9387	27.16	4395	0.4395	1264	8.71	850.0	5.86
1A1P4P4T	Par, AG	AG (vs.) WG	0.229	4.4031	30.36	4535	0.4535	1034	7.13	914.4	6.30
1A1P4P6T	Par, AG	AG (vs.) WG	0.229	4.2779	29.50	3235	0.3235	2306	15.90	1224.9	8.45
		Ave			28.24	4228	0.42		9.71		6.49
		S.D.			2.17	585	0.06		4.12		1.22
1A1T2L1T	Trans, WG oriented spec but crack prop in AG diection	AG (vs.) WG	0.229	4.1687	28.74	3027	0.3027	3219.6	22.20	1309.7	9.03
1A1T2L3T	Trans, WG	AG (vs.) WG	0.229	4.4717	30.83	4876	0.4876	1056.5	7.28	1056.5	7.28
1A1T2L5T	Trans, WG	AG (vs.) WG	0.229	3.9849	27.47	4279	0.4279	800.1	5.52	846.0	5.83
1A1T3L1T	Trans, WG	AG (vs.) WG	0.2295	4.8925	33.73	4651	0.4651	972.8	6.71	1019.0	7.03
1A1T3L3T	Trans, WG	AG (vs.) WG	0.2295	4.6835	32.29	3595	0.3595	1963.1	13.54	1228.3	8.47
1A1T3L5T	Trans, WG	AG (vs.) WG	0.2295	4.8169	33.21	5188	0.5188	946.3	6.52	879.0	6.06
		Ave			31.05	4269	0.43		10.29		7.28
		S.D.			2.51	819	0.08		6.50		1.27

2.3.1.2 Graphite Knowledge Base

ORNL staff attended and participated as Committee chairperson and liaison to the Generation IV International Forum Handbook in the IAEA-organized Consultancy Meeting on the Development of a Taxonomy for Nuclear Graphite Knowledge Management: December 14-15, 2017. The purpose of this meeting was to further develop the draft taxonomy for the IAEA Nuclear Graphite Knowledge Base, focused on the proceedings of the annual International Nuclear Graphite Specialists.

The IAEA Nuclear Graphite Knowledge Base seeks to preserve and further expand scientific information on the physical, chemical, mechanical and other properties of graphite relevant for nuclear-power, nuclear-safety and other nuclear-science and technology applications. The data archive it contains has proven invaluable to the nuclear graphite community.

All records associated with the IAEA Nuclear Graphite Knowledge Base are kept on the Nucleus platform based on SharePoint. To add value to the user community, it is important to establish a well-developed taxonomy that will facilitate advanced search functionalities to ensure an improved user interface, especially for non-expert members. A draft taxonomy was developed during a consultancy

meeting in December 2015 and further enhanced by limited internal efforts. It needs to be enhanced and further expanded.

2.3.2 Advanced Graphite Creep Irradiations

2.3.2.1 AGC-3 PIE Data Package

PIE testing of irradiated graphite samples from the third AGC-3 was completed in December 2017. AGC-3 is the third in a series of six irradiation test trains planned as part of the AGC experiment to fully characterize neutron-irradiation effects and radiation-creep behavior of current nuclear graphite grades to moderate dose levels (≤7 dpa). All data from the PIE testing were reported in the ART Level 2 Milestone (M2NT-18IN060504031), "Complete AGC-3 Post-Irradiation Examination Data Package," issued December 5, 2017. The data are being uploaded into the ART Nuclear Data Management and Analysis System (NDMAS) database and will be transferred to the Generation IV International Forum Handbook later in the year.

The AGC-3 capsule marks a new milestone in the AGC experiment because the graphite samples were irradiated to temperatures nominally 250°C higher than the previous AGC-1 and AGC-2 capsules. AGC was irradiated to a nominal temperature of 820°C and to a peak dose of 3.7 dpa. As with previous AGC capsules, half of the AGC-3 specimens were subjected to compressive stresses to induce irradiation creep. Irradiated testing included specimen dimensions for both stressed and unstressed specimens to establish the irradiation creep rates and mass and dimensional data necessary to derive density, elastic constants (Young's modulus, shear modulus, and Poisson's ratio) from ultrasonic time-of-flight velocity measurements, Young's modulus from the fundamental frequency of vibration, electrical resistivity, and thermal diffusivity and thermal expansion data from 100 to 650°C. A complete evaluation of trends in the material property changes and irradiation-induced creep is currently underway and will be reported in future AGC-3 post-irradiation examination analysis reports.

A limited comparison of the data between pre- and post-irradiation properties was undertaken to ensure that property measurements exhibiting values significantly higher or lower than the average were not a measurement error. These limited summaries of the data are shown below in Figure 15 through Figure 20.

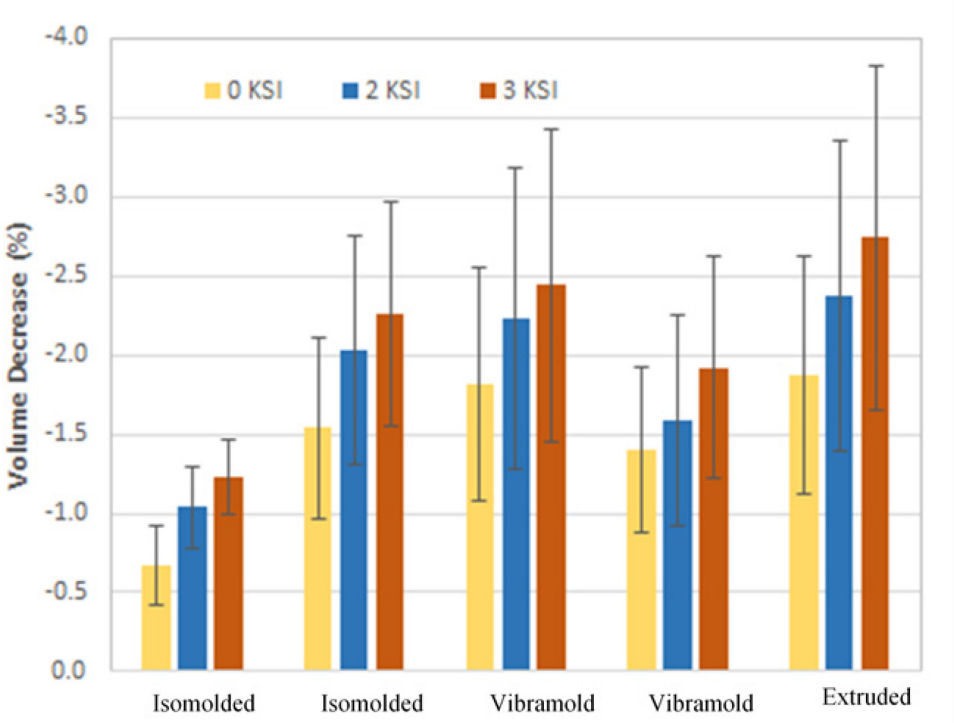

Figure 15. Volume decrease due to irradiation creep for five major grades of graphite.

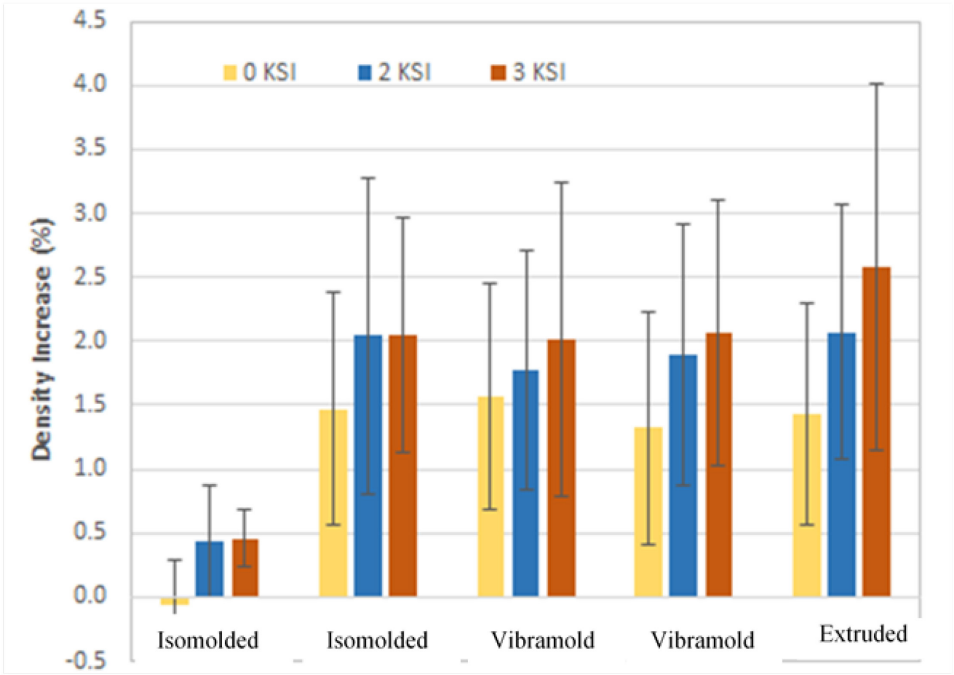

Figure 16. Density increase due to irradiation volume shrinkage for five major grades of graphite and three stress conditions. Error bars represent one standard deviation in the percent density increase.

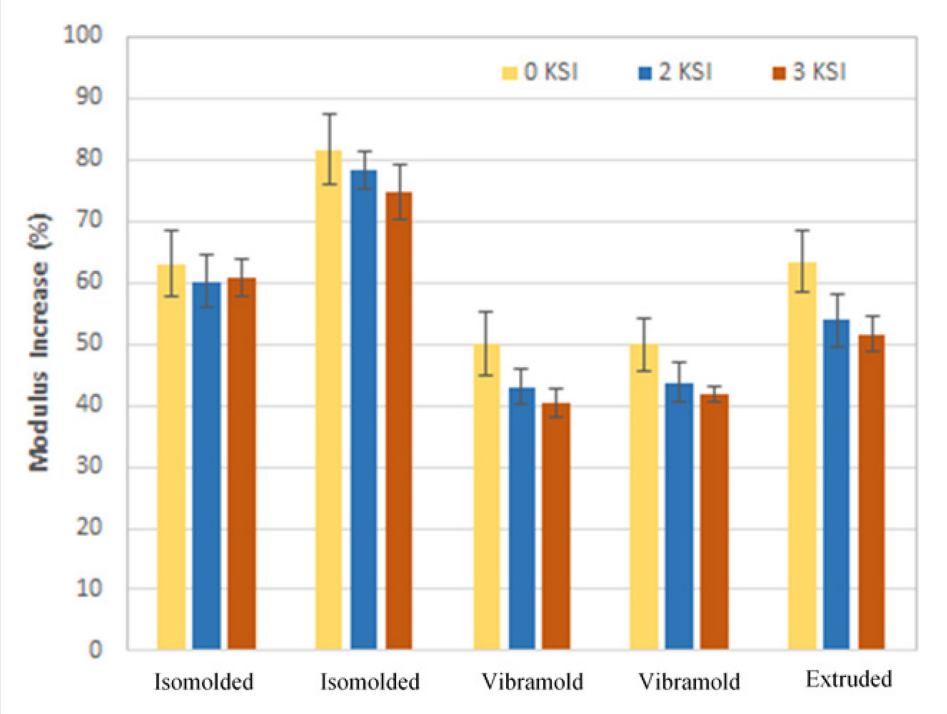

Figure 17. Young's modulus derived from the measurement of fundamental frequency for five grades of graphite and three different stress conditions.

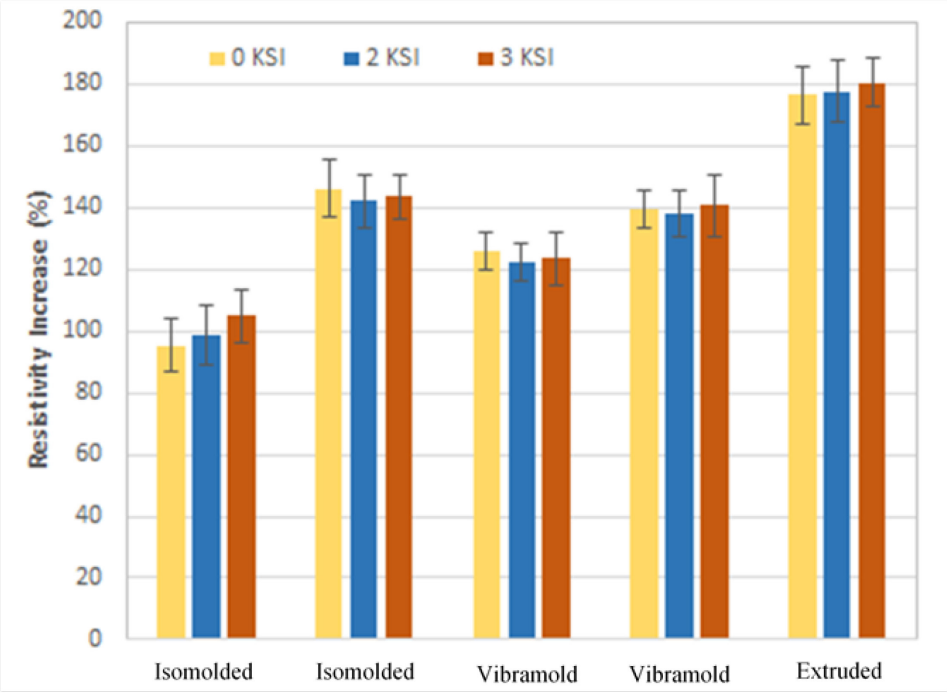

Figure 18. Electrical resistivity for five grades of graphite and three different stress conditions.

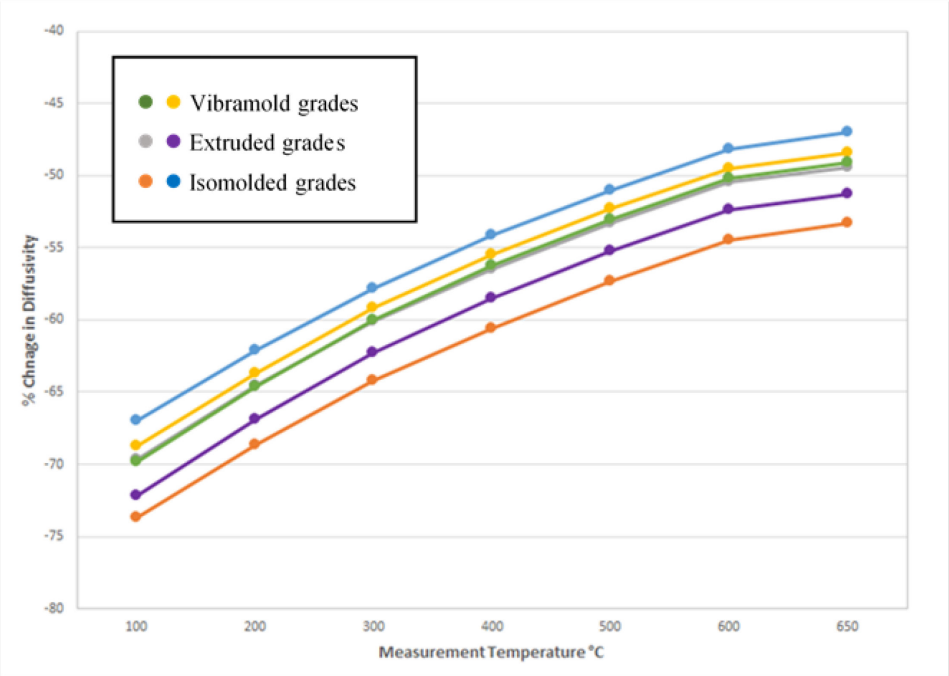

Figure 19. Percent change in diffusivity as a function of measurement temperature for six grades of graphite.

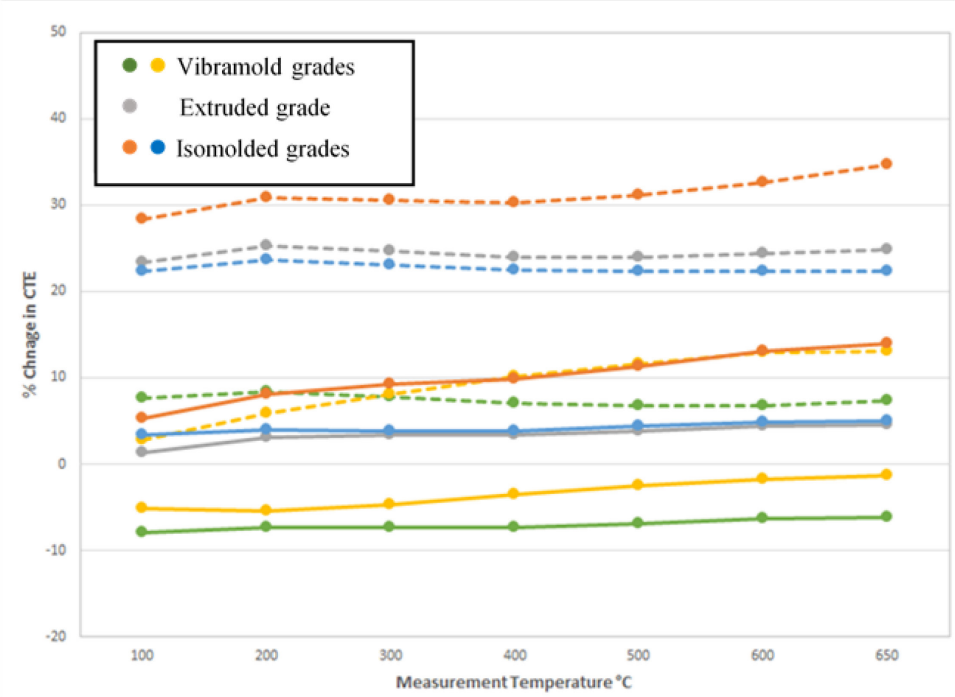

Figure 20. Percent change in coefficient of thermal expansion (CTE) for five different grades of graphite as a function of temperature for stressed and unstressed conditions.

Thermal creep of graphite (international collaboration with Manchester University)

In support of an international collaboration with Manchester University, long-term (>750 hour) thermal creep studies are being performed at INL on three nuclear-graphite grades, comprising IG-110 (fine grain isomolded), NBG-18 (medium grained vibrational molded), and Gilsocarbon (preferred grade for the AGR reactors in the U.K.). To date, INL has completed thermal creep at two different temperatures (2500°C and 2000°C) and is currently completing the lower-temperature creep studies at 1500°C. Manchester is conducting XRD studies on the crept samples to determine internal crystallographic changes during thermal creep. This will complement the INL thermal creep studies, which analyze the defect-microstructure changes during thermal creep as compared to the irradiation creep changes to similar strain levels.

Preliminary results from the INL studies demonstrate the similarities of changes to the material properties after thermally induced and irradiation-induced strain. Both thermally induced and irradiation-induced strains produce large increases to the CTE in a range of nuclear-graphite grades. This implies that microstructural changes in the graphite are contributing the change in CTE for nuclear-graphite grades in addition to irradiation damage. Further results from post-strain analysis from INL and Manchester studies should allow determination of the contributions from crystallographic changes, microstructure-defect changes, and irradiation damage.

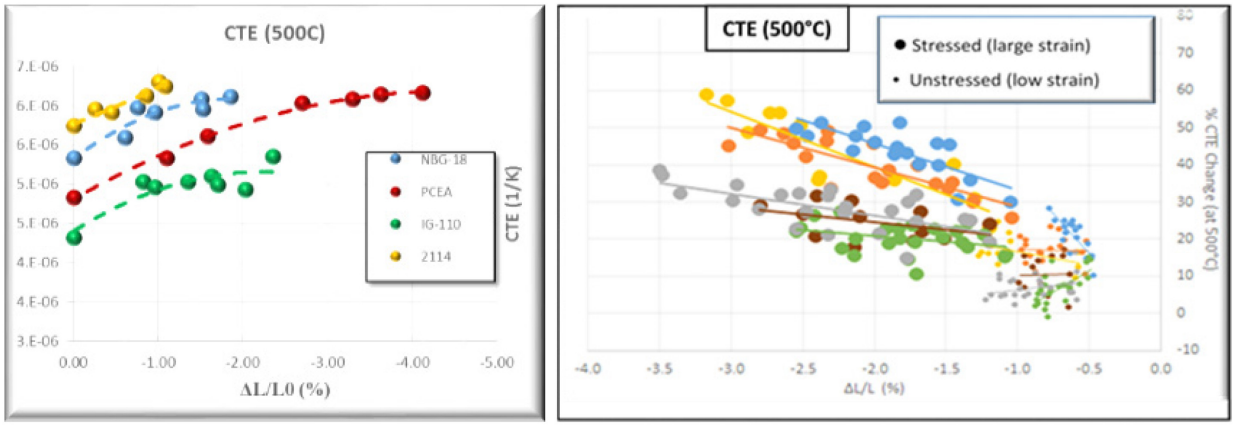

Figure 21. CTE with thermally induced and irradiation-induced strain for four grades of graphite.

2.4 Design Methods and Validation

2.4.1 Experiments and Computational Fluid Dynamics Validation

2.4.1.1 High-Temperature Test Facility

Ten redesigned heater rods were received, and benchtop testing began. The ball-in-socket design has performed well, with little change in resistance between a vertical stack and a stack with some lateral translation. The measured resistance is higher than desired, so new rodlets with larger ends and thicker cylindrical bodies have been ordered.

Test acceptance reports for the shakedown tests and the three other matrix tests were prepared and issued. The reports and associated data have been sent to INL.

2.4.2 Physics Methods

An accurate, high-resolution full-core model of prismatic high-temperature reactors for burnup and transient analysis remains a challenge for both reactor analysts and computer codes. The cores are spatially large, but some features are quite small (TRISO particles, burnable poison [BP] pellets). The treatment of both neutron scattering in graphite and resonance capture are complex and not adequately

captured using the methods traditionally used in HTGRs and commonly used in light-water reactors (LWRs). For transient analysis, temperature feedback is a function of the TRISO fuel form, but full-core models cannot resolve phenomena at this scale without careful averaging over space and energy. For burnup calculations, a second (pin) level of heterogeneity must be resolved to capture the local effects of BPs and fuel pins while accurately propagating their effects through and between blocks.

The OECD MHTGR Benchmark is being used at INL to drive the development of full-core and transient models and for code-to-code verification against other methods. The IAEA CRP on HTGR Uncertainty Analysis in Modeling is likewise being developed to compare the propagation of uncertainties in lattice and full-core modeling. The tools developed in these activities are being used in related HTGR support work, for example in the joint modeling of the high-temperature test reactor with the Japan Atomic Energy Agency under the ART Civil Nuclear Energy Research and Development Working Group funding. Existing lattice tools (e.g., DRAGON, HELIOIS, SERPENT, and SCALE) have different strengths and weaknesses, and concurrent modeling with these tools helps to identify code and model discrepancies, sensitivities, and best practices.

2.4.2.1 OECD/NEA MHTGR-350 Benchmark.

INL leads an international prismatic HTGR benchmark for comparing and evaluating lattice and core analysis codes, based on the 350-MW MHTGR design information obtained from General Atomics (GA). Similar to the PBMR-400 Transient Benchmark sponsored by the OECD NEA, this OECD/NEA benchmark is a multiyear (2013–2018) project that has already yielded a set of reference steady-state and lattice problems that can be used by DOE, the Nuclear Regulatory Commission, and vendors to assess their codes. The OECD/NEA sponsorship of the prismatic benchmark is valuable because it attracts international participation and leverages benchmark expertise and publishing apparatus already used for other LWR, sodium fast reactor, and high-temperature reactor development programs.

This benchmark activity is now being completed, with data submitted for Phases I and III currently being compared. Four comparison reports were issued at the end of December (as a single Level 3 milestone) for each of the three exercises of Phase I, as well as the lattice results for Phase III. The Phase II transient cases have so far only been completed by INL and were reported in 2015. It will be proposed to the OECD/NEA working group at the review meeting in February that Phase II either be renamed to Phase III, or removed from the specifications since no other transient results are likely to be produced. Due to the limited distribution of these documents (because they are still under review by the OECD/NEA before being released to the public domain), only an overview of the main findings for Phases I and III is provided in the sections that follow.

For the stand-alone neutronics Exercise 1, it was found that the results show good agreement among the various models. The transport solvers produce eigenvalues that are ~190 pcm above the diffusion solutions for both homogenizations, and when diffusion and transport eigenvalues are evaluated together the standard deviation (SD) is within 100 pcm of the mean.

The type of control rod (CR) homogenization used does not have a large effect on the eigenvalue due to the shallow insertion of the CR bank in this configuration, but the worth of the CR is very sensitive to the CR homogenization, with 275 pcm higher CR worth using the one-sixth CR homogenization. The transport solvers calculate a CR worth that is 30 pcm above that of the diffusion estimate. The relative SD (RSD) in the calculation of the CR worth is less than 1% for the independent solver groups, diffusion and transport, but the combined statistical values are within 1.7%.

CR homogenization had a significant effect on power distribution. Full homogenization overpredicts the radially averaged power on the top of the core by 5% and underpredicts the power at the bottom of the core by -2.6%. The relative power difference show a maximum difference of 23.97% between the two CR homogenizations at the top level of the active core region. The CR homogenization produces thermal flux differences of 22% in the active core.

For the stand-alone thermal fluid Exercise 2, the results show fairly good agreement among the various participants, but not nearly as close as the neutronics results. Fuel-region temperatures compare best because the dominant phenomena is convective heat transfer. In general, average fuel and moderator temperatures matched within an RSD of 2–3%, but larger variances were observed for the maximum fuel temperature (up to 8.2%). Larger discrepancies are also observed in reflector regions, where the codes have modelling differences in flow, conduction, and radiation treatments. In principle, Exercise 2a is the simplest case, with all flow through the core and fixed thermophysical properties, but very large temperature differences (up to 60%) were found in the inner top reflector for this case. This large difference was not observed for the other three exercises, where bypass flows cooled the reflectors, implying that the conduction model and boundary condition used by RELAP5-3D in this region require further investigation. The energy balance and bypass flows achieved by the RELAP5-3D code can also be improved with better convergence of some of the solution fields.

The neutronic results from Exercise 3 show a much larger spread compared to the neutronics standalone Exercise 1. The INL eigenvalue and axial offset values are significantly lower (~2,500 pcm) and higher (by ~20%), respectively, than the other two results. The axial-power density is noticeably more top-peaked in both INL models, but the control-rod worths seem to be unaffected by this difference and are well-matched. As was observed in Exercise 1, the modelling of the CR as homogenized over the full block or just a one-sixth triangle makes a significant difference in CR worth. In contrast to Exercise 1, the effect on the eigenvalue is insignificant (within 27 pcm), demonstrating the nonlinear nature of the temperature feedback.

In general, the Exercise 3 thermal-fluid differences between the participants are similar to the trends identified for the standalone thermal-fluid Exercise 2. Thus, the change from a fixed power density distribution to a coupled nodal kinetics solution did not seem to affect the level of agreement significantly or, stated differently, the large differences inherent in the thermal fluid models dominate smaller differences observed for the neutronics-only models.

Spatial power and temperature distributions differ significantly (more than 20%) in certain regions of the core; especially in the inner, outer and upper reflector regions. Average fuel and moderator temperatures are better matched in the fuel region (generally within ~10%) than in the ex-core reflector regions. The use of a TRISO kernel-temperature model by two of the participants resulted in large differences (up to 200°C or 20%) in the bottom core region, compared to INL models that did not include the modelling of the TRISO fuel particles. Large differences were also found in the modelling of graphite thermal conductivity in the various models, and it is recommended that this aspect be reviewed by the participants. INL models will be reviewed and improved in January 2018, and updated reports will be issued for review by the OECD/NEA committee by the end of February.

For the lattice-level Phase III submissions, it was found that results from the exercises show good agreement between the participants. In the eigenvalue calculations for Exercise III-1 and the main depletion calculations for Exercise III-2, the standard deviations are within 200 pcm. The temperature effect from 300 to 1200 K is 4,385 and 5,553 pcm without and with burnable poisons (BPs), respectively. The BP worth is roughly -8%, which is consistent with other prismatic HTGRs designs. There is good agreement among participants in predicting BP worth.

Significant initial flux and power gradient exist at beginning of life (BOL), with peaking factors ranging from 1.96 to 0.58 across the central fuel block in the cold case with BPs. Higher temperature tends to redistribute power and reduce the power gradient, with peaking factors between 1.72 and 0.58. A consistency in the pattern of the results exists between the cold case, at 300 K, and the high-temperature case at 1200 K. Peaking is much higher without BPs, with maximum values of 2.25 and 1.91 for the cold- and hot-temperature conditions, respectively.

These gradients at BOL are ameliorated during the fuel burnup, leading to power distributions that are quite constant across the central fuel block in comparison. There is good agreement in the compact

peaking factors during the depletion, but agreement deteriorates slightly near end of life (EOL) for cases with and without BPs. All compact power distributions have standard deviations within 2.25%.

The reactivity physical transformation (RPT) method performs well in the computation of integral parameters like reactivity and the worth of BPs, albeit with a significant varying bias. The RPT method does not track well the depletion of ^{238}U or the production of higher actinides. The ^{241}Am concentration is poorly predicted in Serpent during depletion. Other issues with fission-product production are observed in various codes, with ^{85}Kr being the largest source of discrepancy.

2.4.2.2 IAEA CRP on HTGR Uncertainties.

In many cases, best estimate plus uncertainty analysis of reactors is replacing the traditional conservative (stacked uncertainty) method for safety and licensing analysis. The use of a more fundamental methodology is also consistent with the reliable high-fidelity physics models and robust, efficient, and accurate codes available today. To facilitate uncertainty analysis applications, a comprehensive approach and methodology must be developed and applied. HTGRs have their own peculiarities, including coated-particle design, large graphite quantities, different materials, and high temperatures that require simulation techniques not utilized in LWR analysis. The IAEA launched the CRP on the HTGR Uncertainty Analysis in Modeling in 2013 to study uncertainty propagation in the HTGR analysis chain. Two benchmark problems are defined, with the prismatic design represented by the General Atomics (GA) MHTGR-350 and a 250-MW modular pebble-bed design similar to the HTR-Pebble Bed Module (PM)(INET, China). INL is leading the prismatic-reactor problem specification of Phases I through III. The IAEA recently approved an extension of this CRP to September 2019.

A draft Level 3 milestone report was submitted to for review by the CRP working group at the end of August 2017 on the comparison results obtained for Phase I of the prismatic reactor design cases, based on the 350-MW GA MHTGR. Phase I includes the data sets received for the neutronics cell (Exercise I-1), lattice (Exercise I-2a, b), and supercell (Exercise I-2c) exercises; steady-state (Exercise I-3) and transient (Exercise I-4) thermal fluids exercises; and experimental validation case based on the Very High Temperature Reactor Critical Assembly (VHTRC) facility. An updated version was subsequently released at the end of November, incorporating the comments received by the Gesellschaft für Anlagen- und Reaktorsicherheit (GRS) participant. It is expected that this document will be superseded by a formal IAEA TECDOC publication by mid-2019.

In the first quarter of FY-18, work continued on the specifications for the Phase II steady-state neutronics and thermal fluid cases. The Phase II cases will make use of the propagated lattice cross-section libraries set up by participants during Phase I. The draft specifications will be submitted to the IAEA CRP working group by the end of April as a Level 3 milestone.

3. 90-DAY LOOK AHEAD

3.1 Important Activities

3.1.1 Fuels Development

- Complete cleanup run for 1400°C heating test of AGR-3/4 Compact 10-4.
- Complete 1200°C heating test of AGR-3/4 Compact 10-2.
- Ship four AGR-2 Compacts from INL to ORNL.
- Receive defect-induced AGR-2 particles from ORNL to support re-irradiation testing of particles in Neutron Radiography Reactor (NRAD).
- Initiate AGR-2 loose particle ceramography on particles from AGR-2 Compacts 3-3-1, 5-3-3, 5-4-2, and 6-3-3.
- Initiate ceramography of three AGR-3/4 compacts (5-2, 7-2, and 12-2) to observe the morphology of DTF particles.
- Complete gamma counting of the 150 radial deconsolidated particles from AGR-3/4 compact 3-3 in the HOG station.
- Finalize contract for the design and fabrication of the AMIX furnace. The vendor quoted a 19-week delivery time for this effort.
- Continue testing of the benchtop air/moisture-ingress development furnace under air/helium- and steam/helium-mixture conditions.
- Complete the revision to Engineering Calculation and Report ECAR-2574, allowing the use of a titanium irradiation capsule as well as an aluminum irradiation capsule in NRAD.
- Begin development of the Experiment Safety Analysis (ESA) for re-irradiation of AGR compacts in NRAD.
- Complete Hot Cell 5 window replacement at the Analytical Laboratory.
- Resume AGR-3/4 radial deconsolidation operations in Hot Cell 5 at the Analytical Laboratory.

3.1.2 High-Temperature Materials

- Dr. Injin Sah from the Korean Atomic Energy Research Institute will visit INL in mid-February 2018 to plan experiments on creep-fatigue behavior of diffusion bonded Alloy 617 as part of an International Nuclear Research initiative project.
- Staff from INL will participate in ASME Code week in Las Vegas, NV, February 5–7, 2018.
- Staff from INL will participate in a meeting of the Generation IV International Forum VHTR Materials Program Management Board in Sydney, Australia, March 20–23, 2018.

3.1.3 Graphite Development and Qualification

- Additional tensile testing of grade 2114 is expected. This will give enough data to produce Weibull Statistics.

3.1.4 Methods

- Prepare the draft Phase II specifications for the IAEA CRP on HTGR uncertainties for review by the working group at the end of March.

- Issue updates of the OECD/NEA MHTGR-350 benchmark reports for Phase I Exercises 2 and 3, incorporating the latest INL Relap5-3D results.
- Continue benchtop testing of the redesigned HTTF heater rods.
- Obtain and begin installing replacement equipment for HTTF.